

1 Manuscript type: Research article

2 **Assessing Landslide Damming susceptibility in Central Asia**

3 Carlo Tacconi Stefanelli^{a,b,*}, William Frodella^{a,b}, Francesco Caleca^{a,b}, Zhanar Raimbekova^{c,d},
4 Ruslan Umuraliev^e, Veronica Tofani^{a,b}

5 ^a University of Florence, Department of Earth Sciences, via G. la Pira 4, 50121 Florence, Italy

6 ^b UNESCO Chair on the Prevention and Sustainable Management of Geo-Hydrological Hazards, University of
7 Florence, Largo Fermi 2, 50125 Florence, Italy

8 ^c Institute of Seismology of Republic of Kazakhstan (IS), Almaty, Kazakhstan

9 ^d Al-Farabi Kazakh National University, Department of Geography and Environmental Sciences, Al-Farabi ave.
10 71, A15E3C7 Almaty, Kazakhstan

11 ^e Institute of Seismology of the National Academy of Sciences of Kyrgyz Republic (ISNASKR), Bishkek, Kyrgyz
12 Republic

13 * *Correspondence to:* carlo.tacconistefanelli@unifi.it

14 **Abstract**

15 Central Asia regions are characterized by active tectonics, high mountain chains with extreme topography with
16 glaciers and strong seasonal rainfall events. These key predisposing factors make large landslides a serious natural
17 threat in the area, causing several casualties every year. The mountain crests are divided by wide lenticular or
18 narrow, linear intermountain tectonic depressions, which are incised by many of the most important Central Asia
19 rivers and are also subject to major seasonal river flood hazard. This multi-hazard combination is a source of
20 potential damming scenarios which can bring cascading effects with devastating consequences for the surrounding
21 settlements and population. Different hazards can only be managed with a multi-hazard approach coherent within
22 the different countries, as suggested by the requirements of the Sendai Framework for Disaster Risk Reduction.

23 This work was carried out within the framework of the SFRARR Project (“*Strengthening Financial Resilience*
24 *and Accelerating Risk Reduction in Central Asia*”) as a part of a multi-hazard approach with the aim of providing
25 a damming susceptibility analysis at a regional scale for Central Asia. To achieve this, a semi-automated GIS-
26 based mapping method, centred on a bivariate correlation of morphometric parameters defined by a morphological
27 index, originally designed to assess the damming susceptibility at basin/regional scale, was modified to be adopted
28 nationwide and applied to spatially assess the obstruction of the river network in Central Asia for mapped and
29 newly formed landslides. The proposed methodology represents an improvement of the previously designed,
30 requiring a smaller amount of data, bringing new preliminary information on the damming hazard management
31 and risk reduction identifying the most critical area within the Central Asia regions.

32 **1 Introduction**

33 The mountainous areas of the Djungaria, Tien Shan, Pamir and Kopetdag in Central Asia territories are
34 characterized by complex and active tectonic and are the sources of most of Central Asia rivers. A rugged
35 topography along with complex geological structure and high seismicity are ideal setting for large slope failures.
36 In general, when landslides completely obstruct a river channel, they generate a landslide dam whose consequences
37 can be a serious hazard forming upstream backwater and causing catastrophic downstream flooding, changes in
38 the riverbed, embankments instability triggering other landslides with a cascading effect (Swanson et al., 1986;
39 Costa and Schuster, 1988; Casagli and Ermini, 1999). The effects of impounded water and anomalous flood waves,
40 resulting from a dam breach, have significant economic and social impacts in upstream and downstream areas with
41 economic and human losses (King et al., 1989; Dai et al., 2005; Chen and Chang, 2016). Rebuilding costs can be
42 extensive, as they are direct (e.g., infrastructure and buildings reconstruction, safety measures) and indirect (e.g.,
43 loss in real estate value and damage caused to industrial and agricultural production), harder to estimate.

44 Most of landslide dams have a short life as about 40% of them collapse within 24 hours after formation and about
45 80% within one year (Costa and Schuster, 1988; Tacconi Stefanelli et al., 2015; Fan et al., 2020). Given the limited
46 available time, a complete and reliable analysis of the risks, requiring in-depth study of the phenomenon, is not
47 achievable during the event and only rapid assessments for the dam stability are suitable. When the people to
48 evacuate are too many or the related risk is too high, engineering measures for the hazard reduction are attempted:
49 among these are for example modification of slope geometry, drainage, retaining structures and internal slope
50 reinforcement (Popescu and Sasahara, 2009; Schuster and Evans, 2011). Therefore, part of the effects from
51 landslide damming can be avoided or at least reduced thanks to mitigation and prevention measures (e.g., slopes
52 stabilization or re-profiling) if the most critical areas with the highest damming probability are known.
53 Consequently, planning and prevention tools, such as risk and susceptibility mapping, are essential to reduce the
54 costs of natural hazard and improve the efficiency of environmental management.

55 Reactivation of ancient landslides triggered during different climatic and environmental conditions may often
56 generate new mass movements (Casagli and Ermini, 1999; Canuti et al., 2004; Dikau and Schrott, 1999; Borgatti
57 and Soldati, 2010; Crozier, 2010). Landslides generated in the past are often dormant, with strength parameters of
58 the sliding surface close to the residual ones, and difficult to recognize because vegetation, erosion and superficial
59 alteration hide their morphology. Natural causes, such as earthquakes, river undercutting, rainfall, and snowmelt,
60 or even anthropic activity can reactivate these ancient phenomena. Therefore, all dormant landslides capable to
61 reach a river along their pathway can potentially dam it and should be investigated. New landslides, instead, may
62 develop wherever are present suitable conditions along the slopes. The spatial occurrence probability is commonly
63 assessed by landslide susceptibility analysis, highly dependent on landslide volume (Catani et al., 2016), which is
64 difficult to accurately predict.

65 Landslides in Central Asia are quite common and a considerable number of them have huge dimension, often
66 induced by strong earthquakes but also by floods, heavy rainfall and snowmelt (Behling et al., 2014; Golovko et
67 al., 2015; Havenith et al., 2015a; 2015b; 2006b; Kalmatieva et al., 2009; Rosi et al., 2023; Saponaro et al., 2014;
68 Strom and Abdrakhmatov, 2017; 2018). Concerning landslide dam events, in Central Asia regions several mass

69 movements of considerable size produced the obstruction of a river section, of which more than 100 still are
70 existing with a lake (Strom, 2010). Although many of these could be considered stable (Strom, 2010), the
71 occurrence of devastating outburst floods in the last century show that their potential hazard should never be
72 overlooked also considering the seismicity of the region. In the Rushan and Murgab districts of Gorno-Badakhshan
73 Autonomous Oblast (Pamirs, Tajikistan) along the Murghab river, the Usoi landslide dam is one of the most
74 famous of the many cases in the regions. Its impounded lake, called Lake Sarez, is 60 km long with 500 m of depth
75 and has a stored volume of about 17 km³, representing the world deepest landslide-dammed lake (Costa and
76 Schuster, 1991; Fan et al., 2020). It was originated on February 18th, 1911, when a MW 7.2 earthquake triggered
77 a giant wedge-failure of about 2.2 km³ of rock (mainly quartzite, schist, shale and dolomite) and debris that blocked
78 the Murgab River and a tributary valley, forming the 560 m high, 5 km long and 4 km wide Usoi dam, impounding
79 Lake Sarez, also creating the smaller Lake Shadau (Strom, 2010).

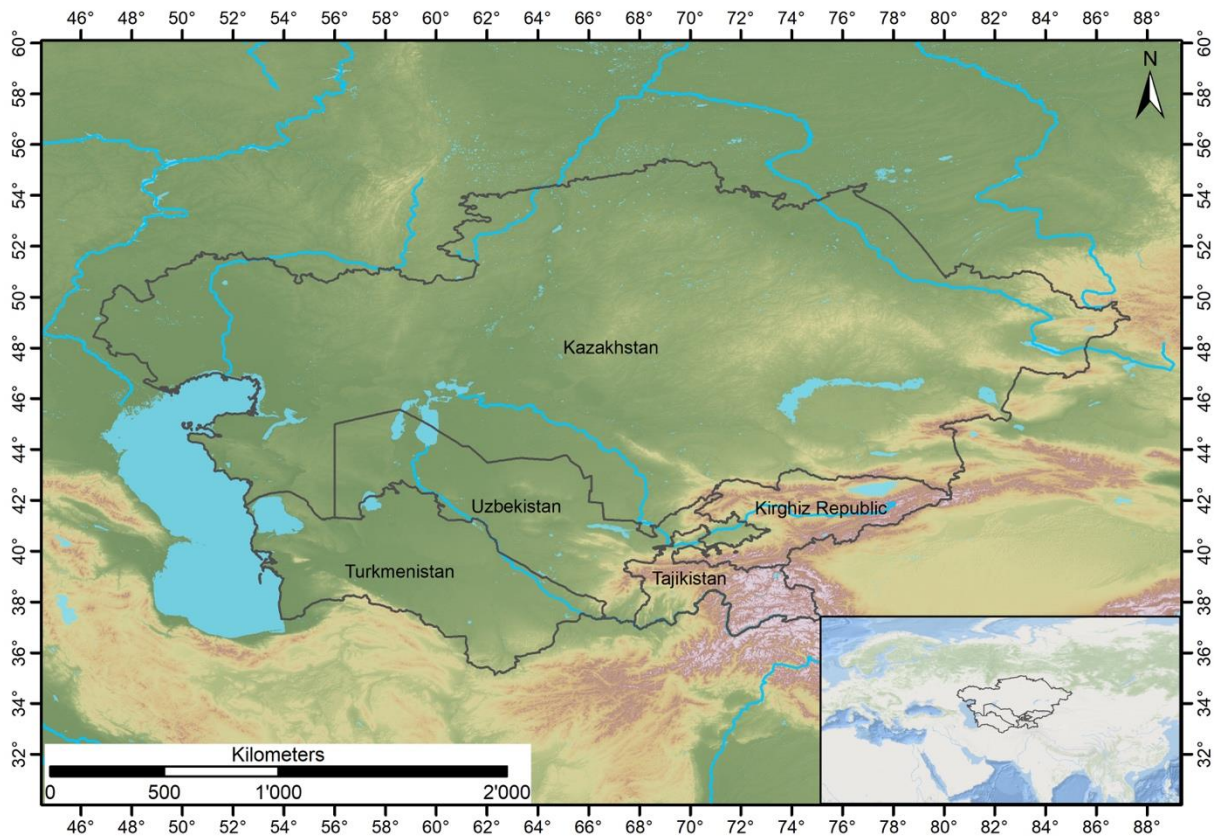
80 Landslide dam evolution, according to some studies (Swanson et al., 1986; Ermini and Casagli, 2003; Dal Sasso
81 et al., 2014; Tacconi Stefanelli et al., 2016), can be estimated through geomorphological indexes which require
82 parameters characterizing the landslide (or the dam) and the river (or the lake). Geomorphological indexes are a
83 powerful classification tool, but their prediction power depend mainly on long studies, a large amount of data and
84 measurement efforts given their empirical nature. Many of these indexes need parameters not always available and
85 easy to acquire, such as grain size distribution (Liao et al., 2022) or landslide velocity (Swanson et al., 1986).

86 In this work, we propose a simple semi-automatic GIS-based mapping methodology to verify the damming
87 susceptibility of river networks at national scale from existing and neo-formed landslides trough a
88 geomorphological index. This activity research was carried out in the framework of the SFRARR Project
89 (*“Strengthening Financial Resilience and Accelerating Risk Reduction in Central Asia”*) as a part of a multi-hazard
90 approach (Peresan et al., 2023).

91 The proposed mapping methodology represents an innovation in terms of application simplicity, availability of
92 data and of extension of the analysed area, bringing new information on the damming hazard in the Central Asia
93 regions where the landslide susceptibility is quite high (Rosi et al., 2023) and a set of input data required for the
94 methodology application were available.

95 **2 Study area**

96 Central Asia is a region of vast diversity encompassing high mountain chains, deserts, and steppes (Figure 1). The
97 southern and eastern parts of the region are predominantly occupied by the mountainous areas of Djungaria, Tien
98 Shan, Pamir, Kopetdag, and a small part of Western Altaj, with peaks exceeding 7,000 m above sea level (a.s.l.)
99 (Strom, 2010). These intraplate mountain systems, developed in the Cenozoic as a result of the India-Asian
100 collision, is located between the Tarim Basin and the Kazakh Shield (Molnar and Tapponier 1975, Abdrakhmatov
101 et al., 1996; 2003; Zubovich et al., 2010; Ullah et al., 2015). This study focusses the attention on the territories of
102 Central Asia that includes Turkmenistan, Kazakhstan, Kyrgyz Republic, Uzbekistan, and Tajikistan, covering a
103 surface of more than 4·10⁶ km². Mountain building began in the Oligocene (Chedia, 1980) or later (Abdrakhmatov
104 et al., 1996), resulting in a complex system of basement folds interrupted by several thrusts and reverse faults with
105 lateral offset of important amounts (Delvaux et al., 2001).



106

107 **Figure 1. Geographical framework of the study area.** Lake’s polygons from Esri, Garmin International, Inc.;

108 topographic base from NASA’s SRTM project (Far and Kobrick, 2000).

109 The mountain belts contain several regional fault zones (Figure 2), and others cross the mountain systems with a

110 NW-SE axis (Trifonov et al., 1992). Paleozoic crystalline rocks form, for the most part, the mountain ridges which

111 correspond to a neotectonic anticline and are separated by tectonic depressions, with lenticular or linear shapes.

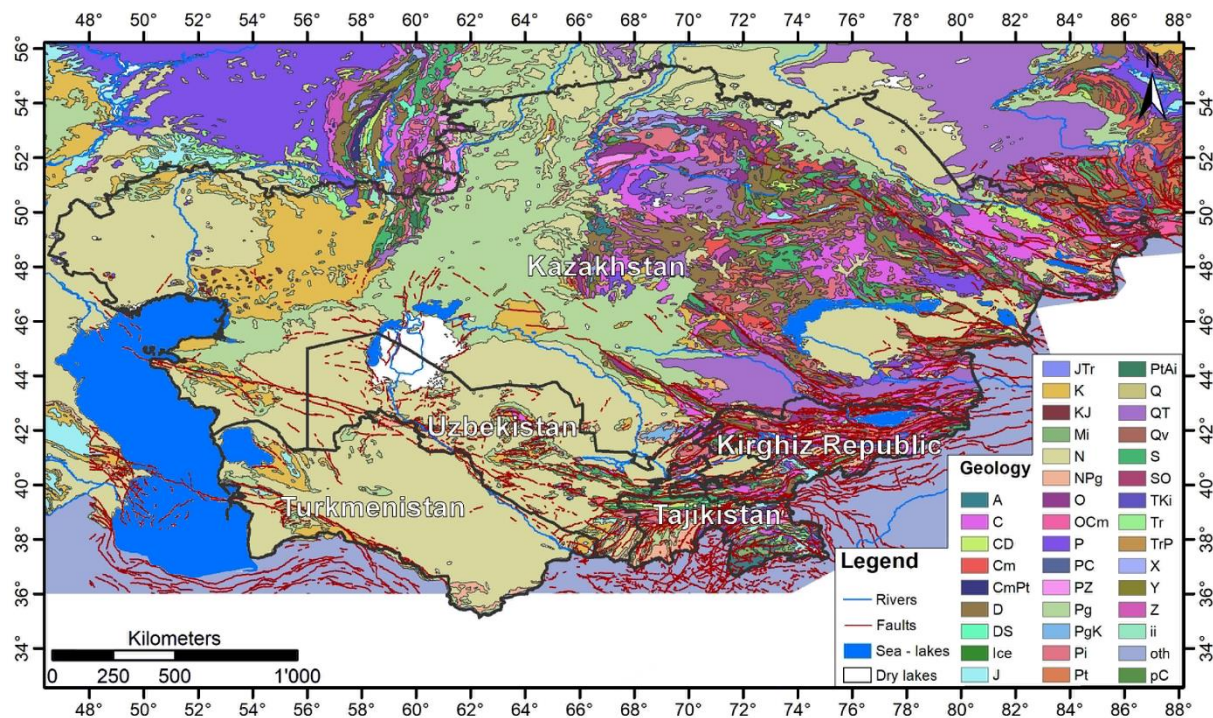
112 These intermountain depressions host the primary river valleys and are filled by Neogene and Quaternary deposits,

113 principally sandstones, siltstones interbedded by gypsum, and conglomerates (Strom and Abdrakhmatov, 2017).

114 Lithologies from Mesozoic and Paleogene are characteristic of the areas at the foot of mountain ranges (Figure 2).

115 This main deeply incised river network, fed by glaciers, snowmelt water and rain, is linked by narrow deep gorges

116 up to 1-2 km deep (Strom and Abdrakhmatov, 2018) and is the origin of most of the rivers in Central Asia.



117

118 **Figure 2. Geological map of the area.** Geological formation data are from the United States Geological Survey
 119 (USGS) (Persits et al., 1997, for the legend), faults are from the Active Faults of Eurasia Database (AFEAD)
 120 (Styron and Pagani, 2020).

121 The retreat and shrinkage of glaciers in Central Asia regions induced by the global warming produce a seasonal
 122 variation in river discharge and consequently an increase of its induced hazards such as Glacial Lake Outburst
 123 Floods (GLOFs) (Falátková, 2016), resulting in countless losses of human life and destroyed infrastructure
 124 (Kropáček et al., 2021; Petrov et al., 2017; Wang et al., 2013). The high seismicity, frequent floods and a complex
 125 geological and topographical structure (such as lithological predisposition, faulting zones, steep slopes) contribute
 126 to predispose the region to frequent landslides which can potentially obstruct the narrow valleys of the mountain
 127 ranges and in turn be the cause of chain risks (CAC DRMI, 2009; Havenit et al., 2017).

128 3 Materials and Methods

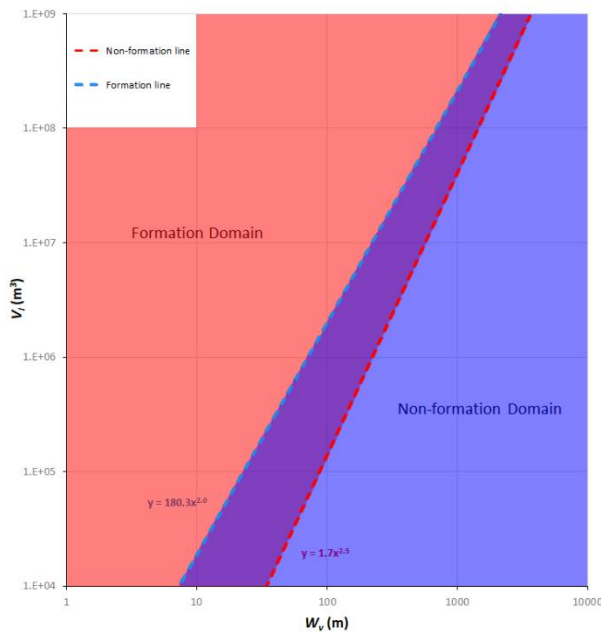
129 The Morphological Obstruction Index (MOI) (Tacconi Stefanelli et al., 2016) is a bivariate index able to evaluate
 130 the potential hazard posed by landslide dams that requires only simple morphometrical parameters which are easily
 131 extracted from common Digital Elevation Models. The MOI is based on the interpolation of 351 documented cases
 132 and has been used in several studies, such as in Italy and Peru (Tacconi Stefanelli et al., 2016; 2018), to assess
 133 landslide damming susceptibility showing better results than others popular indexes (Swanson et al., 1986). This
 134 empirical index is a useful tool for identifying high-risk areas and for prioritizing mitigation efforts in landslide-
 135 prone regions.

136 The MOI is calculated by dividing the volume of the landslide, V_l (m^3), by the width of the river valley, W_v (m),
 137 at the dam location.

138 $MOI = \log \left(\frac{V_l}{W_v} \right)$ (1)

139 The MOI is based on the principle that the higher the ratio of the landslide volume to the river width, the greater
 140 the potential for dam formation. It is important to point out that river width, W_v , shall be defined as the width of
 141 the river valley which can potentially be obstructed creating a dammed lake and not of just the channel where the
 142 river flows, as is often misinterpreted, although in narrow mountain valleys these often coincide.

143 Landslide dams analyzed by the index can be grouped within three evolutionary classes: formed (the red area,
 144 where the plotted landslides have completely blocked their river), not formed (the blue area, where only cases of
 145 unobstructed rivers are found) and of uncertain evolution (the purple area, in which both cases of formed and
 146 unformed dam can be found). The limits of these domains are depicted by two lines, the lower red “Non-formation
 147 line” and the upper blue “Formation line” (Figure 3) obtained by the interpolation of the cases analyzed by Tacconi
 148 Stefanelli et al. (2018).



149
 150 **Figure 3. Schematic plot of the non-Formation line and Formation line.**

151 The equation of the former is expressed as follows:

152 $V_l' = 1.7 \cdot W_v^{2.5}$ (2)

153 Where V_l' is the “Non-formation volume” and is the minimum landslide volume able to potentially block a river
 154 with a given width W_v . Smaller volumes cannot completely dam the river. The latter expression draws the upper
 155 limit for not formed dams and is expressed as follows:

156 $V_l'' = 180.3 \cdot W_v^2$ (3)

157 Where V_l'' is the “Formation volume”, is the minimum landslide volume able to dam the river valley, with a
 158 confidence of 99%, and the inferior boundary of the Formation domain (which includes only formed dams).

159 Intermediate cases that fall between the two lines cannot be confidently identified as formed or unformed and are
160 therefore classified as having uncertain evolution.

161 As originally proposed by Tacconi Stefanelli et al. (2020), these two equations, Eq.(2) and (3), can be used to
162 apply a simple semi-automatic methodology in order to verify at basin scale the damming susceptibility from
163 existing and neo-formed landslides. The following semi-automated procedure, inspired by the one of Tacconi
164 Stefanelli et al. (2020) of which this represents an improvement, is applied on a national scale and can be
165 reproduced entirely in a GIS (Geographic Information System) environment. However, the method, being initially
166 designed for analysis at basin/region scale, applied to such a small scale (national) will not be able to provide
167 detailed information. For this reason, this study represents a preliminary phase of investigation which will allow
168 to concentrate further detailed analysis on the areas identified as more critical.

169 Within an even medium-long time interval the valley width in each river stretch does not change significantly and
170 can be considered an immutable factor in the MOI equation (Eq.(1)). Starting from this assumption, along with
171 Eq. (2) and Eq. (3), if the average river width W_v of each river stretch can be assessed, the two threshold landslide
172 volumes V_1' (Non-formation volume) and V_1'' (Formation volume) can be estimated for each river stretch.

173 Landslides that cause river obstruction are in many cases reactivations of ancient movements that are still in a
174 condition of partial instability and that have not reached a potential equilibrium reaching the valley floor.
175 Therefore, with a landslide inventory it is possible to assess, with some assumptions and simplifications, which
176 among the mapped landslides are able to dam the river section. Each landslide that is not already laying in the
177 valley floor with a volume bigger than V' and V'' are identified as potentially prone to block the river in the future
178 in that point. Then, a "Map of Damming Susceptibility" for reactivation of existing landslides can be generated.

179 The likelihood prediction for new landslides, with volume bigger than V_1' and V_1'' , is a much more difficult task
180 as the volume is a complex value to be estimated (Catani et al., 2016). The exceeding probability of landslide
181 volume used by Tacconi Stefanelli et al. (2020) was reached thanks to the knowledge of the alpha exponent of the
182 statistical frequency distribution of the landslide volumes in the whole study area. To achieve this, a database of
183 landslides with a very high number of events (tens or even hundreds of thousands) should be available (Catani et
184 al., 2016), which in our study area unfortunately is not. To have an assessment of the damming susceptibility for
185 neo-formed landslides the two volume threshold values, evaluated for all the river networks, can be used as well.
186 After estimating the river width of every river stretches, the V_1' and V_1'' values of each of them can be computed
187 through the corresponding two equations. In this way there will be two reference values to be able to assess whether
188 the volume of a new landslide can potentially obstruct an affected river stretch.

189 The input data needed for the procedure are a Digital Elevation Model, a vector layer of the river network, and an
190 updated landslide inventory. The data quality and resolution such as the landslides inventory completeness, the
191 river network reliability and the DEM's pixel size heavily affect the quality of the result (Tacconi Stefanelli et al.,
192 2020). Thus, it was decided to use the DEM with the higher resolution freely available from the NASA's SRTM
193 project (Far and Kobrick, 2000) with a 1 arc-second, or about 30 meters of resolution. The river network came
194 from Coccia et al. (2023). The latter input data is a database of 8910 landslides, that is a compilation of several

195 different inventories collected through decades of field surveys, studies and remote sensing analysis in the study
196 area, shown in Figure 4.

197 Hereafter the detail of each inventory:

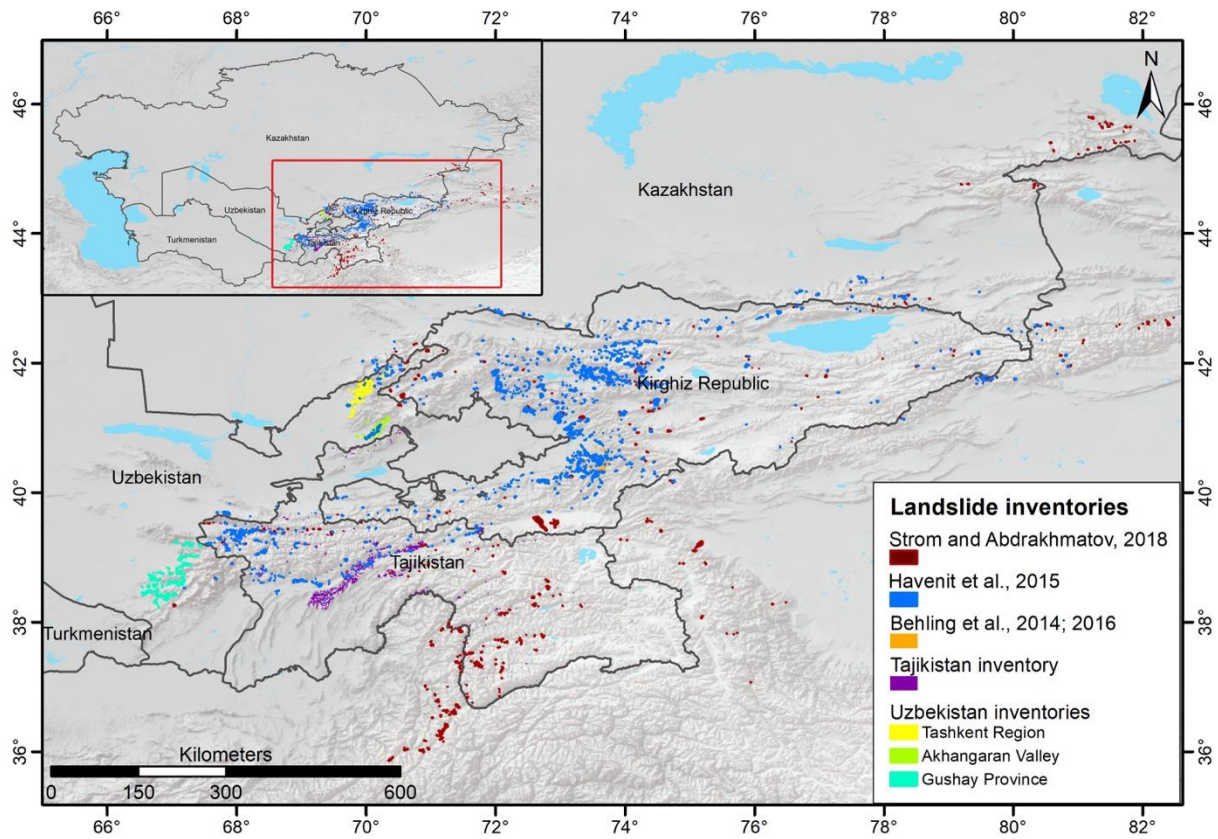
198 • The “Rockslides and Rock Avalanches of Central Asia” (Strom and Abdrakhmatov, 2018): an inventory
199 including more than 1000 of very big ($\geq 1 \text{ Mm}^3$) rockslides and rock avalanches, covering central Asian countries
200 (excluding Turkmenistan and Altai) and also Chinese Tien Shan and Pamir, and Afghan Badakhshan. Collected
201 in decades of field survey and analysis of aerial/satellite imaging, it includes also information on morphometric
202 parameters (runout, area), dammed lakes, head-scarps, and quantitative characteristics (such as area, volume) for
203 about 600 cases.

204 • The “Tien Shan landslide inventory” (Havenith et al., 2015a): is the biggest database in the study area.
205 Assembled through field work, remote sensing and geophysical data interpretation, it includes the elements of the
206 previous inventory alongside other smaller landslides in soft sediments (Havenith et al. 2006a; Schlögel et al.,
207 2011) for a total of 3,462 landslides polygons, including information on landslide length and area.

208 • The “Multi-temporal landslide inventory for a study area in Southern Kyrgyz Republic derived from
209 RapidEye satellite time series data (2009 – 2013)” (Behling et al., 2014; 2016; Behling and Roessner 2020),
210 includes 1,582 landslide polygons mapped from multi-sensor optical satellite time series data (from 1986 to 2013)
211 over an area of 2,500 km² in the Fergana valley rim in southern Kyrgyz Republic, and include information on
212 landslide activity (area and year of trigger).

213 • The “Tajikistan landslide database” produced by the Institute of Water Problems, Hydropower,
214 Engineering and Ecology of Tajikistan (IWPHE), with 2,710 landslide polygons and 114 landslide-prone areas,
215 including information on landslides length and area.

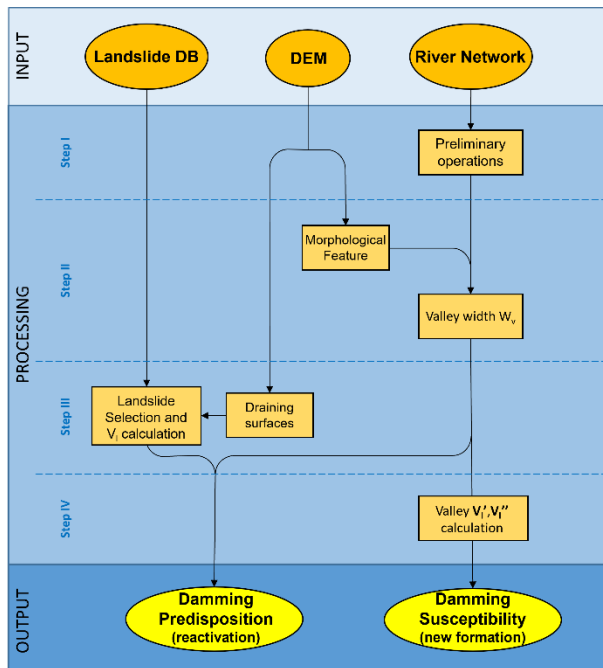
216 • The Institute of Seismology of the Academy of Science of Uzbekistan (ISASUZ) provided an inventory
217 which covers the Tashkent province composed by a point inventory (Niyazov, 2020) and a polygon inventory (345
218 landslide) digitized from the maps in Juliev et al., 2017.



219

220 **Figure 4. Map of the landslide inventories in the study area.** Lake's polygons from Esri, Garmin
 221 International, Inc.; basemap from Esri, USGS, NOAA.

222 The methodology adopted to obtain the maps of damming susceptibility, derived from Tacconi Stefanelli et al.
 223 (2020), is summarized in the following main steps displayed in Figure 5. According to the literature (Swanson et
 224 al., 1986; Fan et al., 2014; 2020; 2021; Tacconi Stefanelli et al., 2015; 2018), river obstructions occur in most of
 225 the time within hilly or mountainous areas and specially along steep slopes. Therefore, considering the extension
 226 of the study area, in order to reduce the time of elaboration and improve the visualization of the results, in step I
 227 of Figure 5 a series of unnecessary data were removed from the calculations during some preliminary operations.
 228 For this reason, river that flow in flat areas (with less than 4° slopes) were not considered in the elaborations, since
 229 their damming probability is certainly very low with an extremely wide valley width. Additionally, to have maps
 230 easier to manage and display, the river network was split in 5 km long river stretches consecutive to each other.

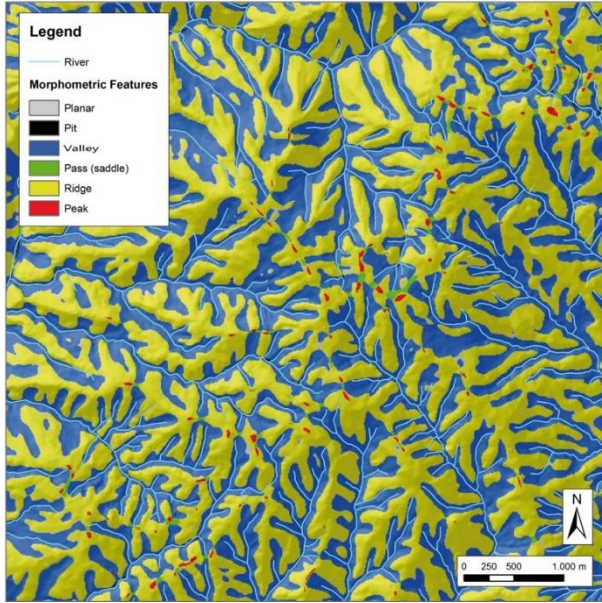


231

232 **Figure 5. Flow chart of the main steps of the mapping methodology.**

233 In applied geomorphology and natural science studies the analysis and characterization of the landscape has
 234 evolved during the last decades with the increasing accessibility of remote sensing data and the development of
 235 different algorithms able to automatically extract morphological features and landform information even at broad
 236 scales (Drăguț and Dornik, 2016; Maxwell and Shobe, 2022; Righini and Surian, 2018; Wang et al., 2010).

237 As already mentioned, the clear definition of the width of a river can be subjective and its measurement difficult
 238 to repeat especially if performed by different operators. In step II of Figure 5, an objective automatic method to
 239 extract morphometrical parameters have been chosen also for this reason. Wood (2009) implemented the
 240 “*LandSerf*” software (already incorporated in SAGA GIS or QGIS software), designed to automatically classify
 241 landforms from DEMs. Similarly for pattern detection and texture analysis within image processing, the software
 242 extracts land-surface parameters (e.g., slope, aspect, and curvature) from DEMs through a multi-scale approach.
 243 During these processing, the algorithm performs a classification of the landscape, grouping the landforms with
 244 homogeneous morphometric characteristics (pits, channels, peaks, ridges, passes, and planes) as shown in Figure
 245 6. Thanks to this algorithm of morphological forms analysis proposed by Wood (2009), the polygons representing
 246 the morphological unit of the river valley can be automatically defined objectively even in a large area and
 247 extracted.



248

249 **Figure 6. Classification of the landscape into morphological classes according to Wood (2009) (modified**
 250 **from Tacconi Stefanelli et al., 2020).**

251 The effectiveness of distinguishing different morphological landforms of this automatic tool is greater in
 252 mountainous regions characterized by significant differences in elevation, compared to flat areas where
 253 distinctions between landforms are less evident. The accuracy of the output is directly correlated with the resolution
 254 of the DEM, which should ideally be about a few meters. Coarser resolutions result in landslide volumes with a
 255 corresponding level of uncertainty.

256 The following phase is to provide to each river stretch a value of a valley width, W_v . A series of 1 km long lines
 257 (hereafter “transects”) are generated, perpendicular to the stretches of the river network, outdistanced by 500
 258 meters apart from each other. The created river valley polygons are used to “cut” the transects and then to measure
 259 the distance between the two river valley borders through the length of the cut transects.

260 Next, the valley widths (W_v) for each segment of the river are determined by assigning them an average value
 261 based on N perpendicular transects, excluding the extreme values (maximum and minimum, respectively W_{max}
 262 and W_{min}), as in the following equation:

$$263 \quad W_v = (\sum_{i=1}^n W_i - W_{min} - W_{max}) \frac{1}{n-2} \quad (4)$$

264 By utilizing an updated database of landslide polygons, in the step III of Figure 5 it is possible to determine if a
 265 reactivated landslide is big enough to cause a complete river blockage thanks to the comparison with the boundary
 266 volumes of V_1' (below which a landslide cannot completely block the river) and V_1'' (above which the river valley
 267 is dammed for sure). A reactivated landslide should follow a downhill path akin to the flow of surface water.
 268 Within each slope, the drainage directions can be easily determined along the river network using a GIS software.
 269 Each mass movement can then be linked to the corresponding river stretch it would reach if reactivated based on
 270 their corresponding draining surfaces.

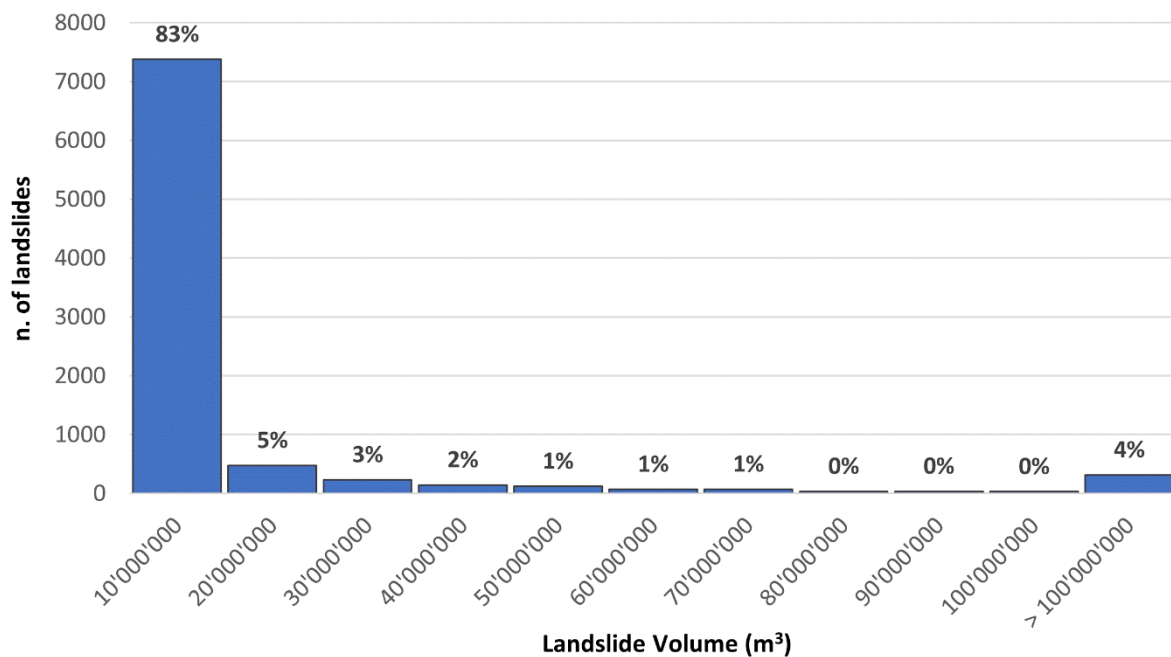
271 Since the information provided by the available inventories in the study area are not homogeneous and comparable,
272 for the computation of the landslide volume were chose to use the areas of the landslide polygons, since it is the
273 most common data. An experimental statistical relationship between areas and volumes was applied:

$$274 \quad V_l = \varepsilon \cdot A_l^\alpha \quad (5)$$

275 where V_l and A_l are respectively the volume and the area of a landslide, ε and α are respectively the constant and
276 the exponent of the power law describing the landslides volumes frequency distribution. Various experimental
277 relations of ε and α have been employed for landslide volume calculations by researchers located in different
278 countries. After an evaluation of these relations in the study area, the parameter proposed by Guzzetti et al. (2009)
279 have been selected because of the number of the studied cases (667) and the magnitude range of the landslides
280 area investigated (from 10^1 to 10^9 m²). The landslide volume computed using this procedure is based on some
281 approximations, since they use geometric simplifications, but it does still reflect the magnitude of the process. The
282 result of the computation in Figure 7 shows an almost bimodal distribution, in which most landslides (83%) have
283 moderate volumes, lower than 10 million m³ (with 63% lower than 1 million m³), but 4% have value higher than
284 100 million m³.

285 Then, Table 1 is used to assign to each landslide of the inventory a classification based on the comparison with the
286 boundary volumes V_1' and V_1'' , with value of 2 if the calculated landslide volume, V_l , is bigger than V_1' (or V_1''),
287 of 0 if it is smaller. For more caution, the V_l values is increased by an arbitrary value of 20% ($V_l \cdot 1.2$) to avoid
288 any potential underestimation during volume estimation and even the possible increase of landslide size with the
289 reactivation due to the mechanism of material entrainment (Hungr and Evans, 2004). For each landslide, if the
290 computed boundary volume V_1' (or V_1'') is bigger than the estimated landslide volume V_l , but smaller than $V_l \cdot$
291 1.2, then a classification value of 1 is attributed.

292 The damming susceptibility of each mapped landslide is assigned by integrating the two comparative classification
293 values from the intensity matrix illustrated in Figure 8. The matrix establishes five qualitative classes on a scale
294 of severity for damming susceptibility, ranging from Very Low (dark green) to Low (light green), Moderate
295 (yellow), High (orange), and Very High (red). The combination of a high V_1'' value (1 or 2) and a lower V_1' value
296 (0 or 1) symbolized by gray squares is not possible according to their respective formulations.



297

298 **Figure 7. Landslide volumes frequency distribution in the central Asia regions.**

299 **Table 1. Comparison table between landslide calculated volumes, V_l , with the boundary volume of Non-**
 300 **formation and Formation, V_l' and V_l'' (after Tacconi Stefanelli et al., 2020).**

	$V_l > V_l' (V_l'')$	$V_l < V_l' (V_l'') < V_l * 1.2$	$V_l < V_l' (V_l'')$
Classification Value	2	1	0

301

$V_l' \backslash V_l''$	0	1	2
0	Very Low		
1	Low	Moderate	
2	Moderate	High	Very High

302

303 **Figure 8. Predisposition matrix used for the assignment of the damming predisposition intensity to the**
 304 **mapped landslides (after Tacconi Stefanelli et al., 2020).**

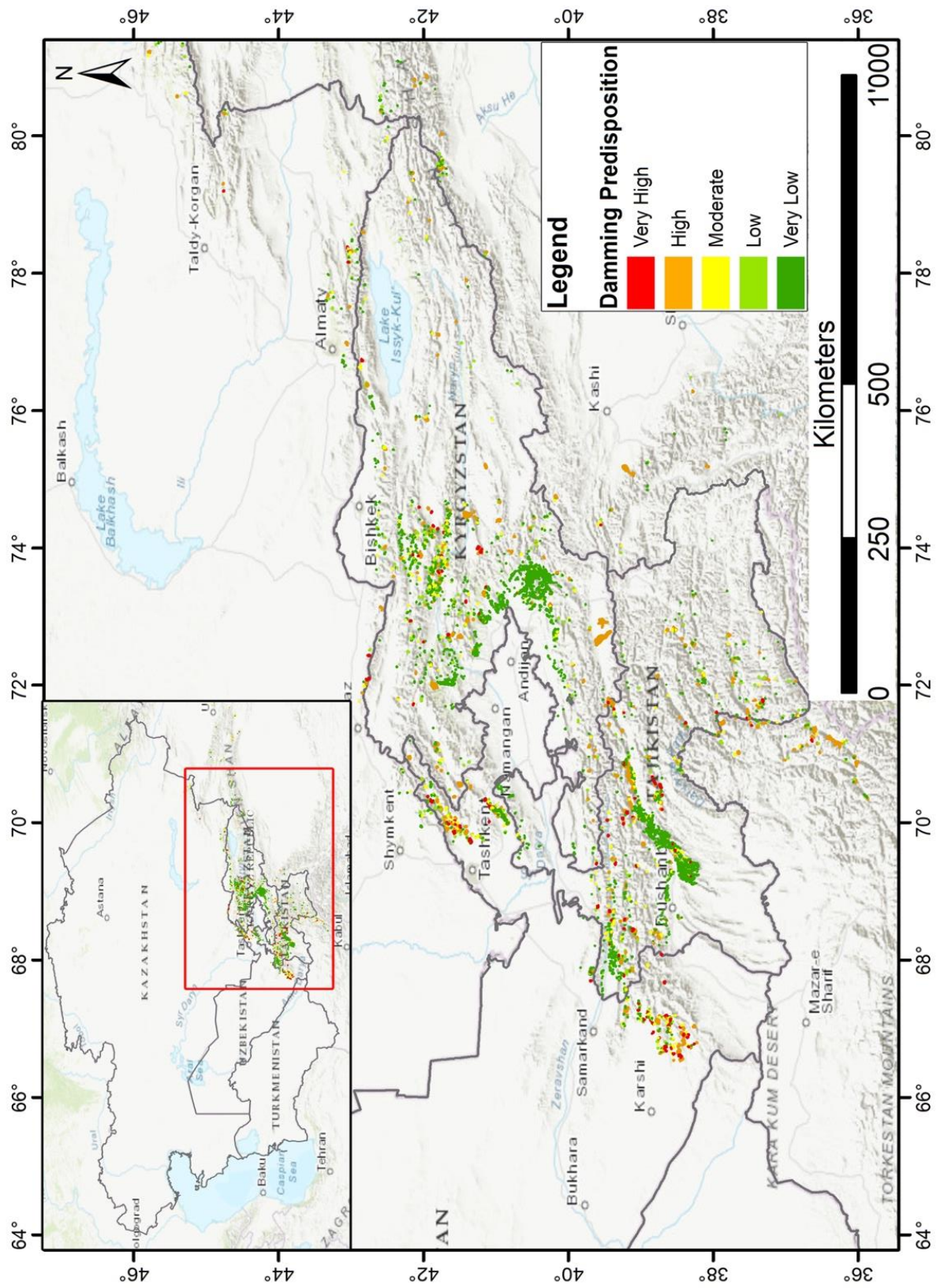
305 Even if the proposed method is objective, it is certainly not free from uncertainties and errors. The 20% increase
306 applied to mapped landslide volumes to reduce underestimation errors can in turn produce false positives for
307 overestimation errors. While a false positive is preferable to a false negative (according to a principle of prudence),
308 too many high-risk false positive cases "spread" an unreal risk throughout the area instead of concentrating it in
309 sites of real risk. Therefore, it can be assumed that the landslide bodies which have previously reached the valley
310 floor have already generated most of their effect on the river network (Strom, 2010) or have had no effect, spending
311 their potential risk component. These landslides, also with a volume higher than V_1' and V_1'' and therefore classified
312 with Very High dam predisposition, even if reactivated probably will not produce any further effect in the future.
313 For these reasons, it was decided to downgrade the classification of those landslides that intersect the river network
314 by reducing its position of the classification of damming predisposition by one class.

315 Using the W_v value for each river stretches estimated during the step III of Figure 5, in the last step (IV) the two
316 boundary landslide volumes, namely "Non-formation volume" and "Formation volume" (V_1' and V_1''), can be
317 estimated by applying the equations of the "Non-formation" (Eq. (2)) and "Formation" lines (Eq. (3)). These two
318 values can be used both to classify the damming susceptibility of the river network (for new landslides) and of the
319 landslides inventory (for their reactivation). For the first case, the computed volume values V_1' and V_1'' embody
320 the required volumes of a new landslide to have a potential or certain (with 99% of confidence) obstruction for
321 each river stretches.

322 **4 Results**

323 The mapping methodology was applied to all the studied territories of the Central Asia region in order to analyze
324 and evaluate the results. Two smaller basins, the upper Pskem river and the Fergana valley, were selected to verify
325 the reliability at a catchment scale of the results obtained from a methodology applied on a national scale. The
326 assessment of damming predisposition on the available landslide inventory on the Central Asia regions is shown
327 in the map of Figure 9, while a closer detail is reported in Figure 11 showing the Kyrgyz Republic territory. The
328 number of landslides (644 cases) classified with Very High damming predisposition from the whole inventory
329 before the class reduction due to the river intersection was unjustifiably and unreasonably large posing excessive
330 concern and risk perception. After the change, this number decreased by 75% up to 166 cases, a high number but
331 more reasonable concerning such a large area. In the class distribution of the damming predisposition shown in
332 Figure 10 the most frequent class is the Very Low, with 81% of the whole database, followed by the Low and
333 High classes both with 6% and the remaining percentage divided among Moderate (5%) and Very High (2%).

334 This distribution is quite coherent with the landslide volumes frequency distribution since it is reasonable to
335 associate landslides with very low volume (83%, shown in Figure 7) with those classified with very low
336 susceptibility (81%, Figure 10). The landslides classified with the higher values of susceptibility (Moderate, High,
337 and Very High with a total of 13%) instead do not only include landslides with higher volumes (more than 100
338 million m^3 representing 4% of the total), meaning that also even smaller landslides can potentially block narrow
339 river stretches in these regions.



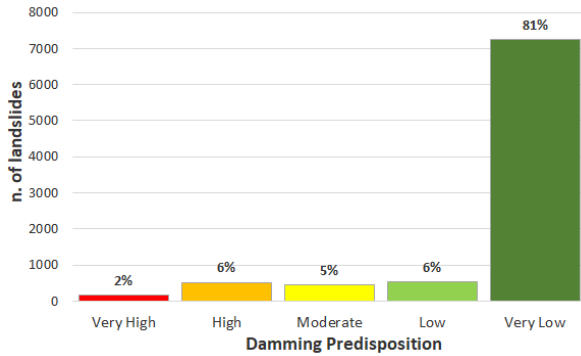
340

341 **Figure 9. Map of Central Asia Landslide Damming Susceptibility.** Basemap source: Esri, HERE, Garmin

342 Intermap, increment P Corp, GEBCO, USGS, FAO, NPS, NRCAN, GeoBase, IGN, Kadaster NL, Ordnance

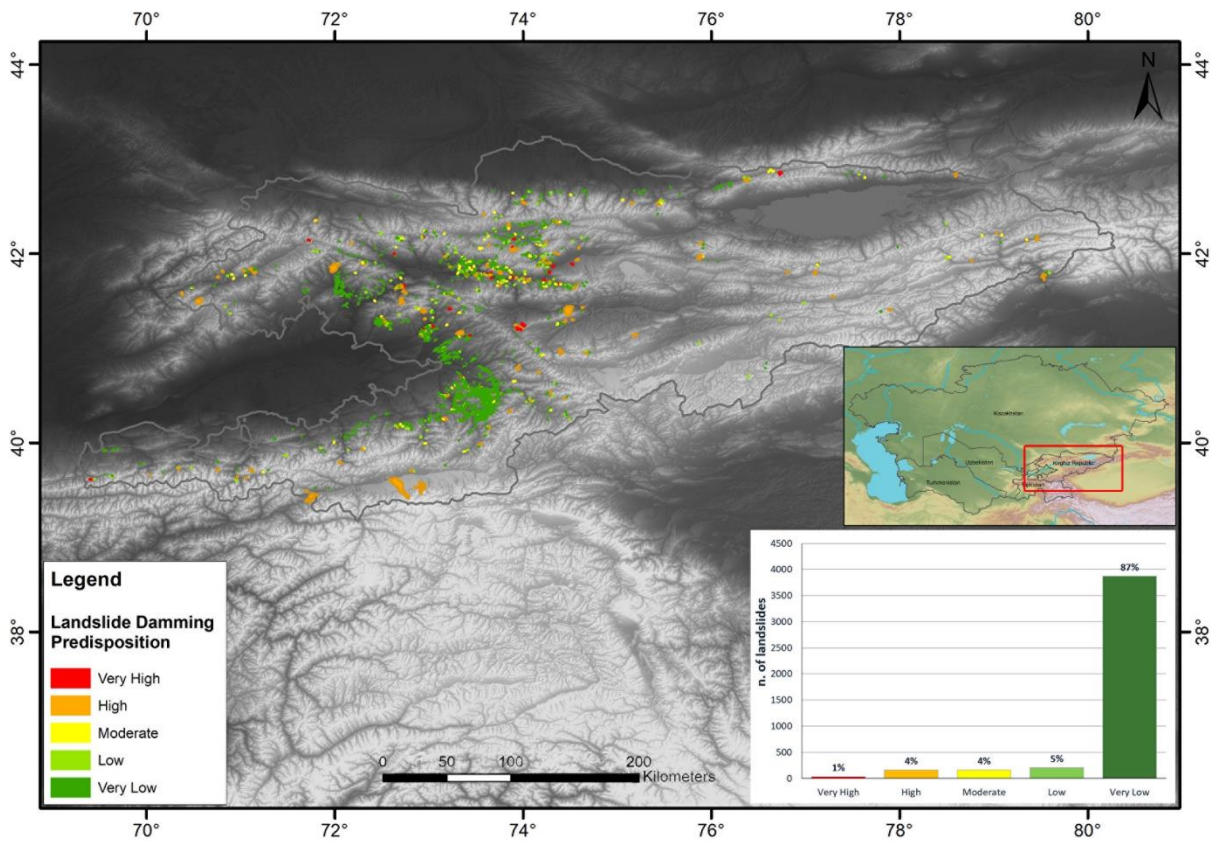
343 Survey, Esri Japan, METI, Esri China (Honk Kong), © OpenStreetMap contributors, and the GIS User
344 Community.

345



346

347 **Figure 10. Classes distribution of the damming predisposition for landslides reactivation.**



348

349 **Figure 11. Map of Damming Predisposition by landslides reactivation in Kyrgyz Republic territory.**

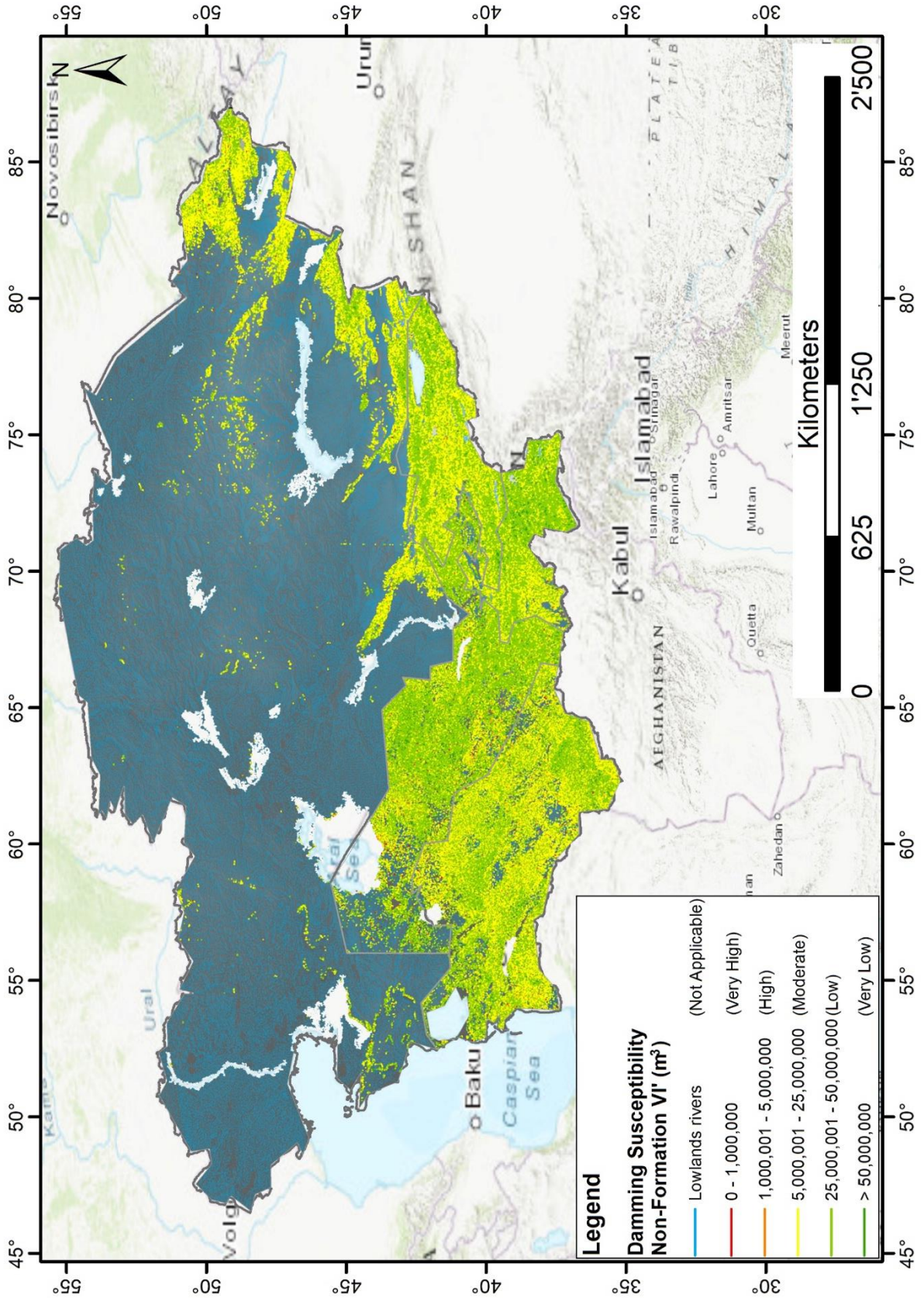
350 Topographic base from NASA's SRTM project (Far and Kobrick, 2000).

351 Concerning the damming susceptibility caused by new landslides along all the river network in the study area, two
352 different maps of the river networks have been produced using the Non-formation and Formation volumes values.
353 Although counterintuitive at first glance, these maps provide complementary information. The former provides
354 the volumes of landslides that surely create an obstruction, while the latter the volumes below which it definitely

355 does not form. According to the preliminary steps of the described methodology, in the river stretches running in
356 flat areas (slope degree less than 4° representing the 88.4% of the entire river network) the analysis has been not
357 applied, due to the extreme unlikelihood that a complete obstruction will occur in such areas. The magnitude of
358 the damming susceptibility of the river networks has been classified in five classes and shown in Figure 12 and
359 Figure 15. The five volumes intervals describing damming susceptibility were decided according to general value
360 distribution of landslides volumes and an expert judgement. Since small landslides are more frequent than large
361 ones, as reported in Figure 7, the lower is the landslide volume required to realize an obstruction, the higher is the
362 magnitude. In the map of damming susceptibility related to the “Non formation”, reported in Figure 12, the central
363 classes, Moderate and Low are the most frequent with 4.4% and 5.8% respectively, as reported in Figure 13. This
364 means that in most of the river stretches in the study area the minimum landslide volume able to potentially dam
365 the riverbed is between the limit values of the two classes, from 2,5 to 25 million m^3 . The following most frequent
366 class is the Very Low with 0.8% and only a very small portion of the river stretches are classified as High and
367 Very High with just 0.4% and 0.2% with a required landslide volume less than 2.5 million m^3 . An example of
368 close-up on the Tajikistan territory is reported in Figure 14.

369 Regarding the map of damming susceptibility related to Formation values, the map in Figure 15 shows slightly
370 different results. The most frequent classes are the two lower ones, Low and Very Low with 4.4% and 6%
371 respectively, as described in Figure 16. Only just the 0.3% and 0.4% fall in the classes Very High and High
372 damming susceptibility. A close-up on the Kyrgyz Republic is reported in Figure 17.

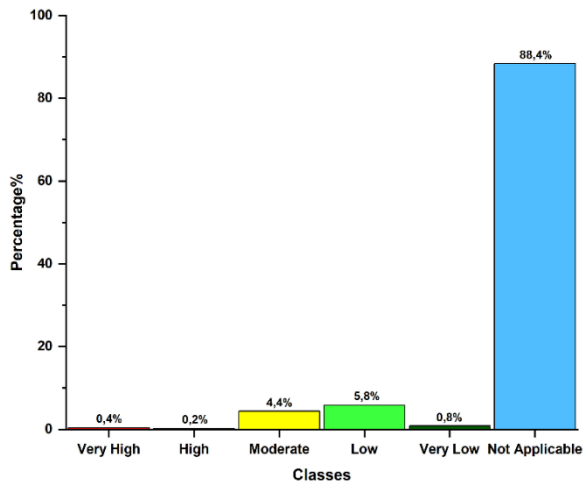
373 The results of the classification for the river networks of each state are shown in Figure 18 to Figure 22. The
374 landslides of Tajikistan, Kyrgyz Republic, Uzbekistan and Kazakhstan regions have been classified according to
375 damming predisposition (Figure 18-a., Figure 19-a., Figure 20-a. and Figure 21-a). In the Turkmenistan territory,
376 it was not possible to assess any damming predisposition by landslides reactivation since the absence of any
377 available landslide inventory. The results of Uzbekistan and Kazakhstan regions (Figure 20-a. and Figure 21-a.)
378 are a bit different from Kyrgyz Republic and Tajikistan regions due to the different availability of landslide
379 inventories and a different orographic and valleys morphology of the formers national territories. As already
380 mentioned, for a clearer comprehension of the damming susceptibility classification of the river network at the
381 national level, the river stretches flowing in lowlands have not been considered in the analysis. Concerning the
382 Damming Susceptibility of Non-Formation (Figure 18-b., Figure 19-b., Figure 20-b., Figure 21-b. and Figure 22-
383 a.), the most frequent are Low and Moderate classes, followed by Very Low class. Fortunately, only very few river
384 stretches have been classified as Very High and High. For the Damming Susceptibility of Formation (Figure 18-
385 c., Figure 19-c., Figure 20-c., Figure 21-c. and Figure 22-b.) most of the rivers fall into Very Low and Low classes,
386 followed by Moderate class. Also in this case, only very few river stretches have been classified as Very High and
387 High. The results of the Tajikistan territory are quite similar to the Kyrgyz Republic and Uzbekistan with which it
388 shares a similar orographic distribution and morphology of the territory. Turkmenistan and Kazakhstan show a
389 slightly different distribution with higher percentage on Moderate class in the Damming Susceptibility of Non-
390 Formation and Low class in the damming susceptibility of Formation.



391

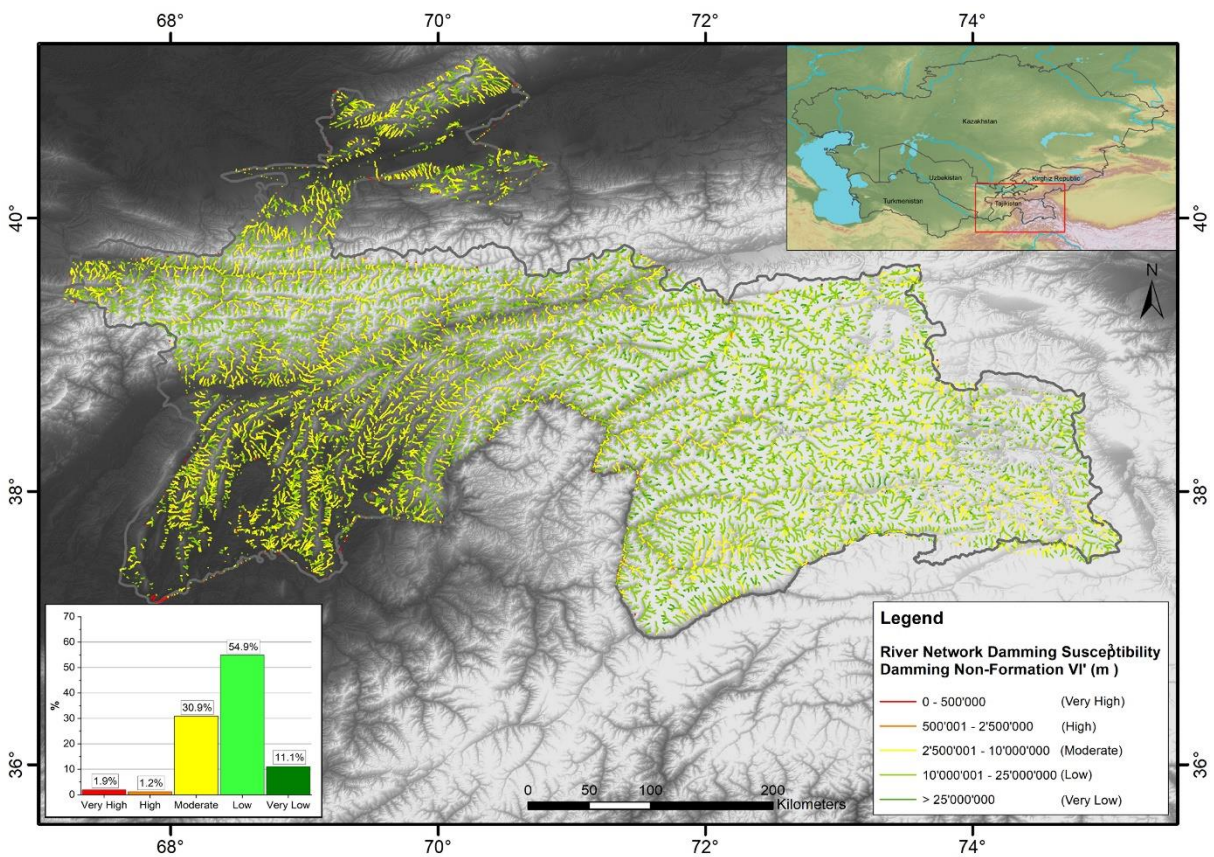
392 **Figure 12. Damming susceptibility map of non-formation of river stretches by new landslides in the**
 393 **region.** River network database from Coccia et al., (2023). Basemap source: Esri, HERE, Garmin Intermap,

394 increment P Corp, GEBCO, USGS, FAO, NPS, NRCAN, GeoBase, IGN, Kadaster NL, Ordnance Survey, Esri
 395 Japan, METI, Esri China (Honk Kong), © OpenStreetMap contributors, and the GIS User Community.



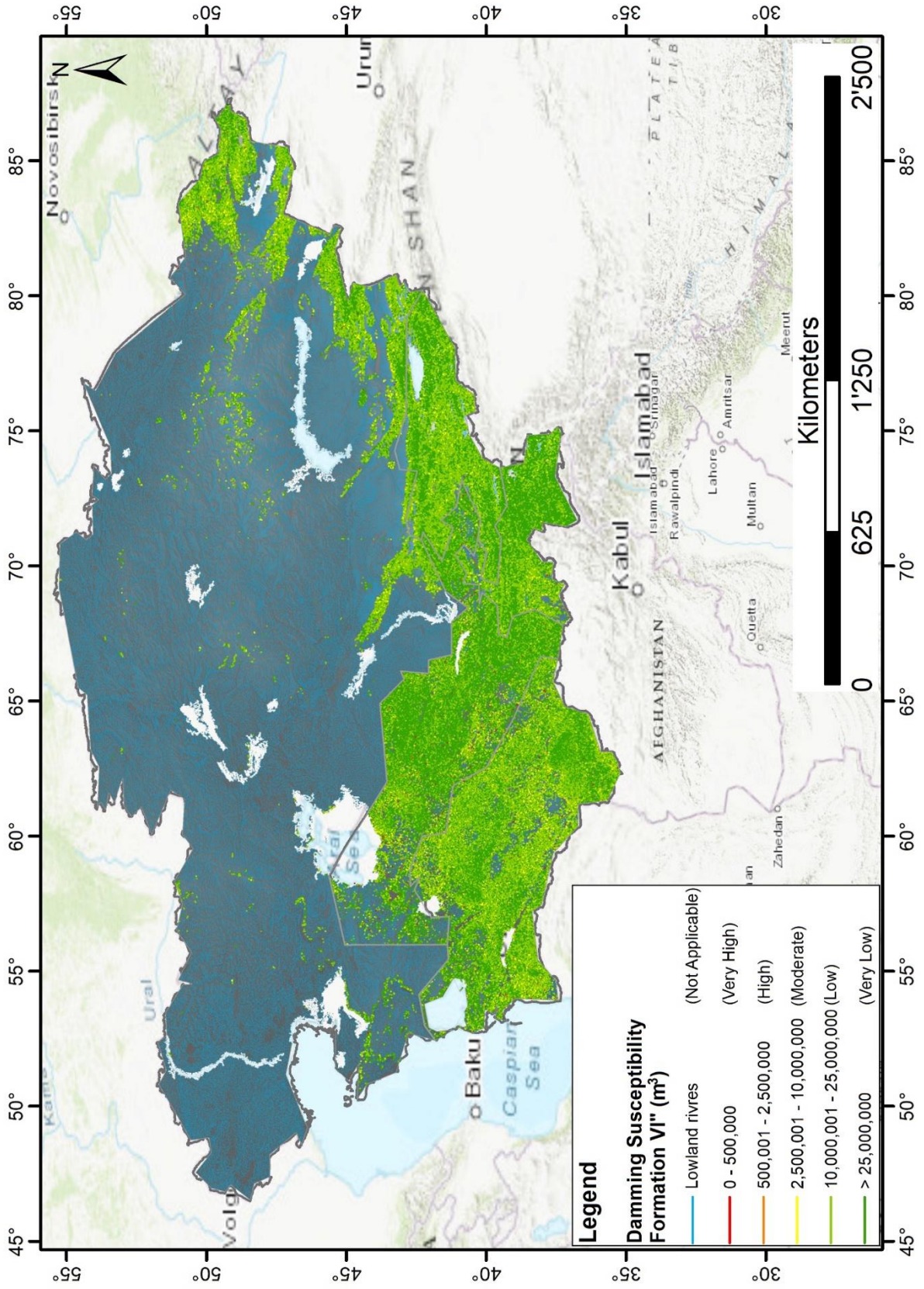
396

397 **Figure 13. Distribution of the damming susceptibility in the study area by new landslides related to Non**
 398 **formation boundary values.**



399

400 **Figure 14. Damming Susceptibility Map of non-formation of river stretches by new landslides in**
 401 **Tajikistan.** River network database from Coccia et al., (2023). Topographic base from NASA's SRTM project
 402 (Far and Kobrick, 2000).



403

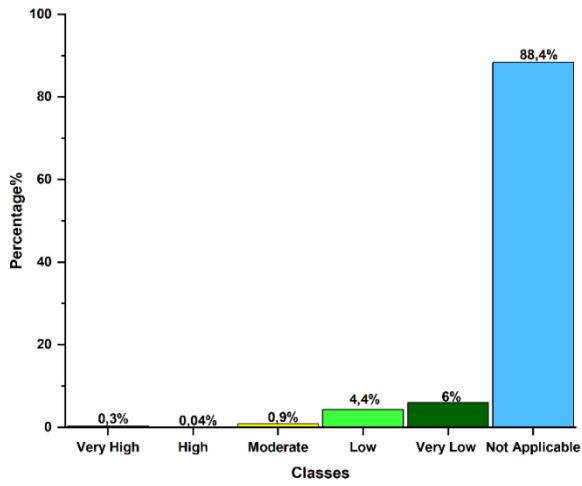
404

Figure 15. Damming Susceptibility Map of Formation of river stretches by new landslides in the region.

405

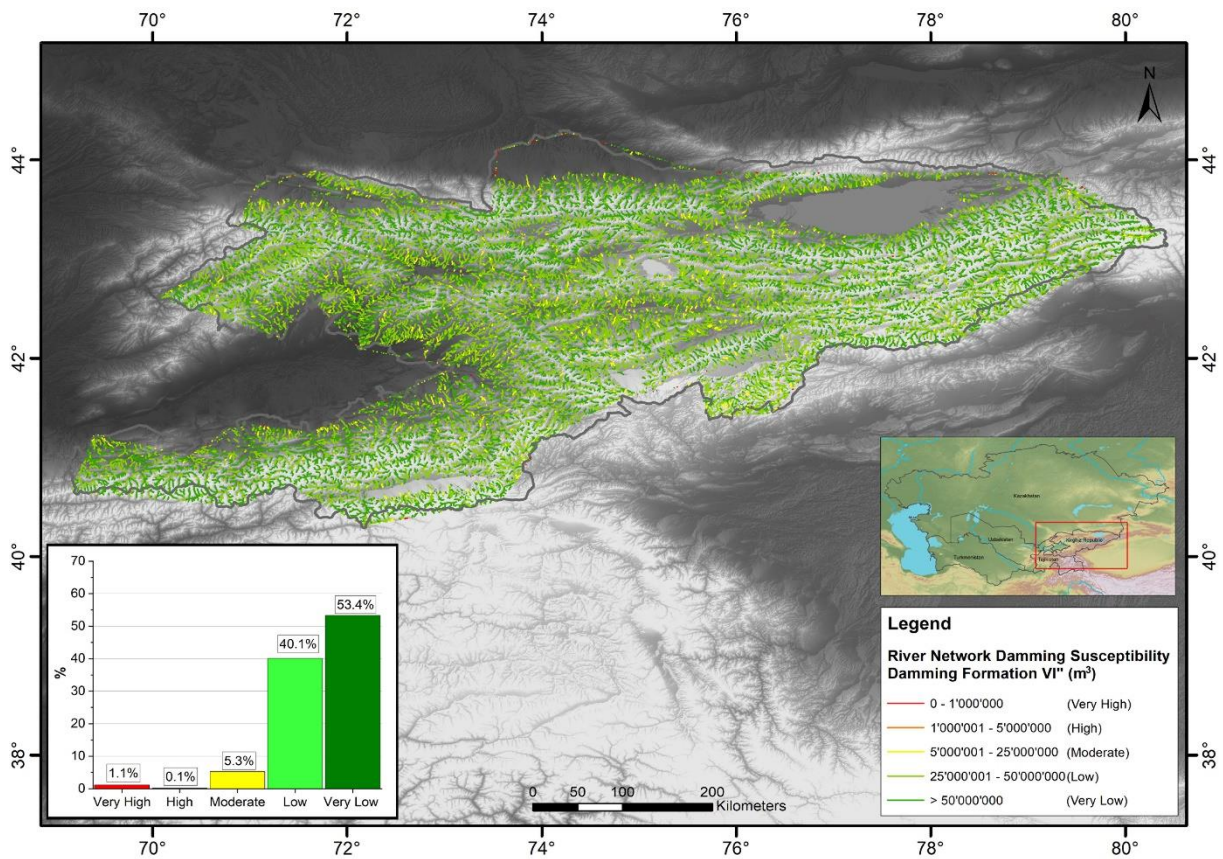
River network database from Coccia et al., (2023). Basemap source: Esri, HERE, Garmin Intermap, increment P

406 Corp, GEBCO, USGS, FAO, NPS, NRCAN, GeoBase, IGN, Kadaster NL, Ordnance Survey, Esri Japan, METI,
 407 Esri China (Honk Kong), © OpenStreetMap contributors, and the GIS User Community.



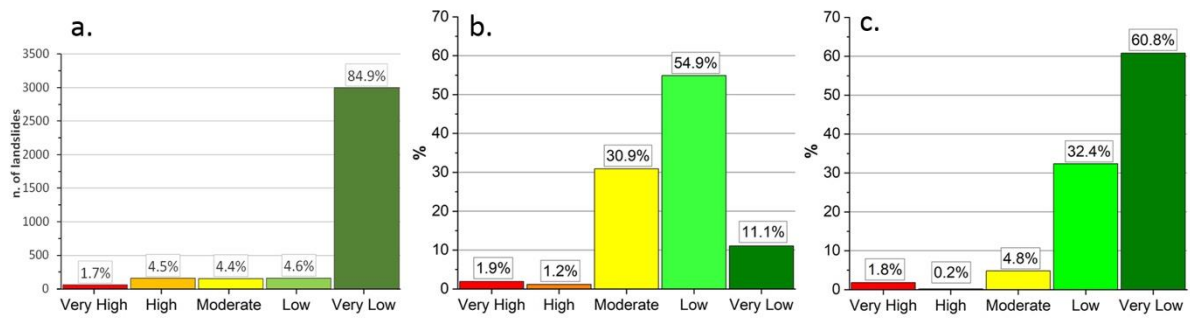
408

409 **Figure 16. Distribution of the Damming Susceptibility in the study area by new landslides related to**
 410 **Formation boundary values.**



411

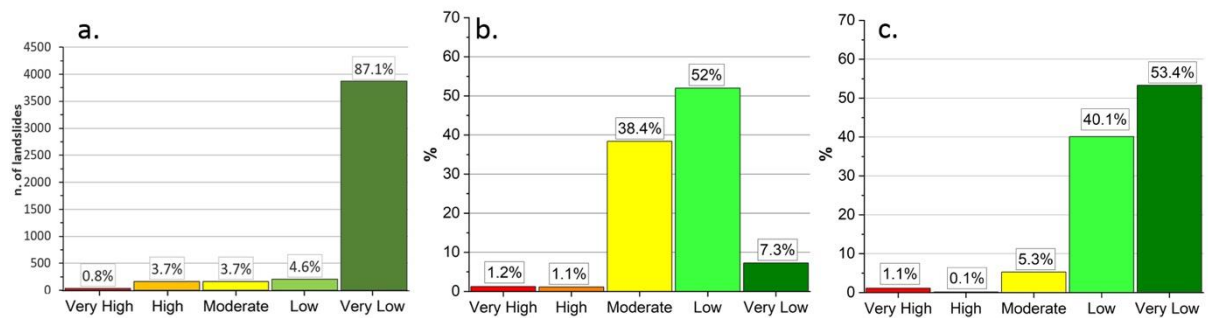
412 **Figure 17. Damming Susceptibility Map of formation of river stretches by new landslides in the Kyrgyz**
 413 **Republic territory.** River network database from Coccia et al., (2023). Topographic base from NASA's SRTM
 414 project (Far and Kobrick, 2000).



415

416 **Figure 18. Classes distribution in Tajikistan of the Damming Predisposition for landslides reactivation**

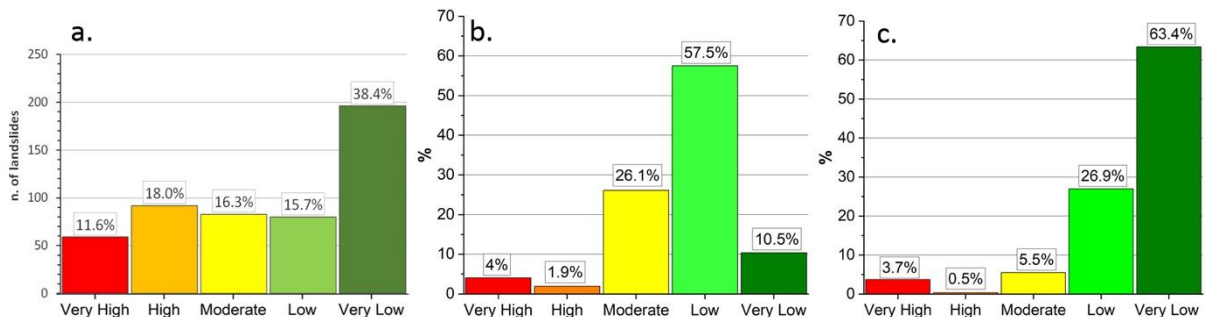
417 **(a.), Damming Susceptibility of Non-Formation (b.) and of Formation (c.) for new landslides.**



418

419 **Figure 19. Classes distribution in the Kyrgyz Republic of the Damming Predisposition for landslides**

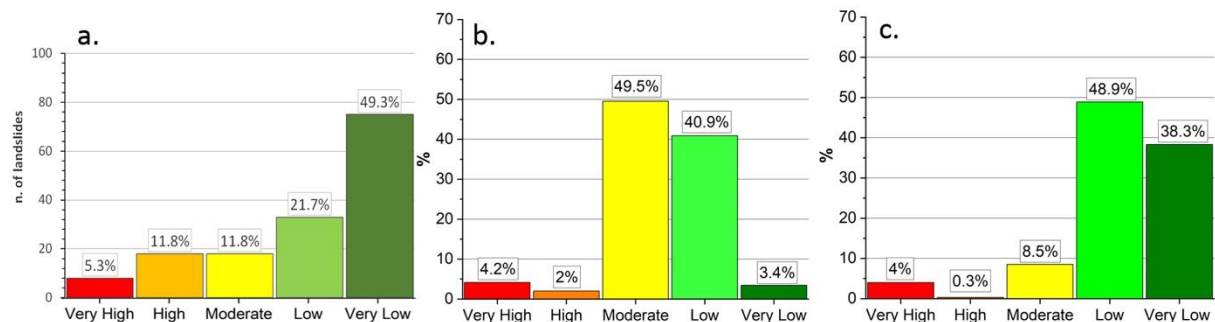
420 **reactivation (a.), Damming Susceptibility of Non-Formation (b.) and of Formation (c.) for new landslides.**



421

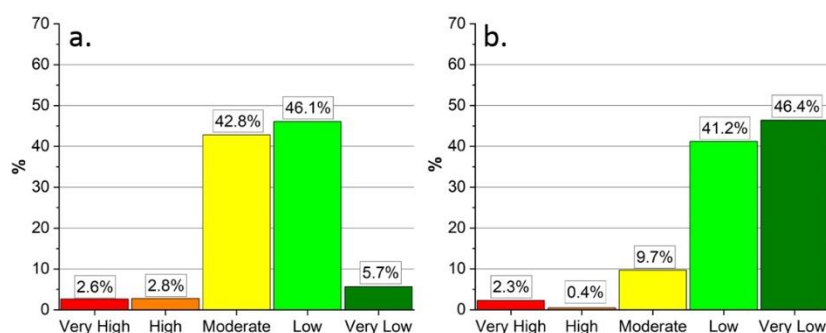
422 **Figure 20. Classes distribution in Uzbekistan of the Damming Predisposition for landslides reactivation**

423 **(a.), Damming Susceptibility of Non-Formation (b.) and of Formation (c.) for new landslides.**



424

425 **Figure 21. Classes distribution in Kazakhstan of the Damming Predisposition for landslides reactivation**
 426 **(a.), Damming Susceptibility of Non-Formation (b.) and of Formation (c.) for new landslides.**



427
 428 **Figure 22. Classes distribution in Turkmenistan of the Damming Susceptibility of Non-Formation (a.) and**
 429 **of Formation (b.) for new landslides.**

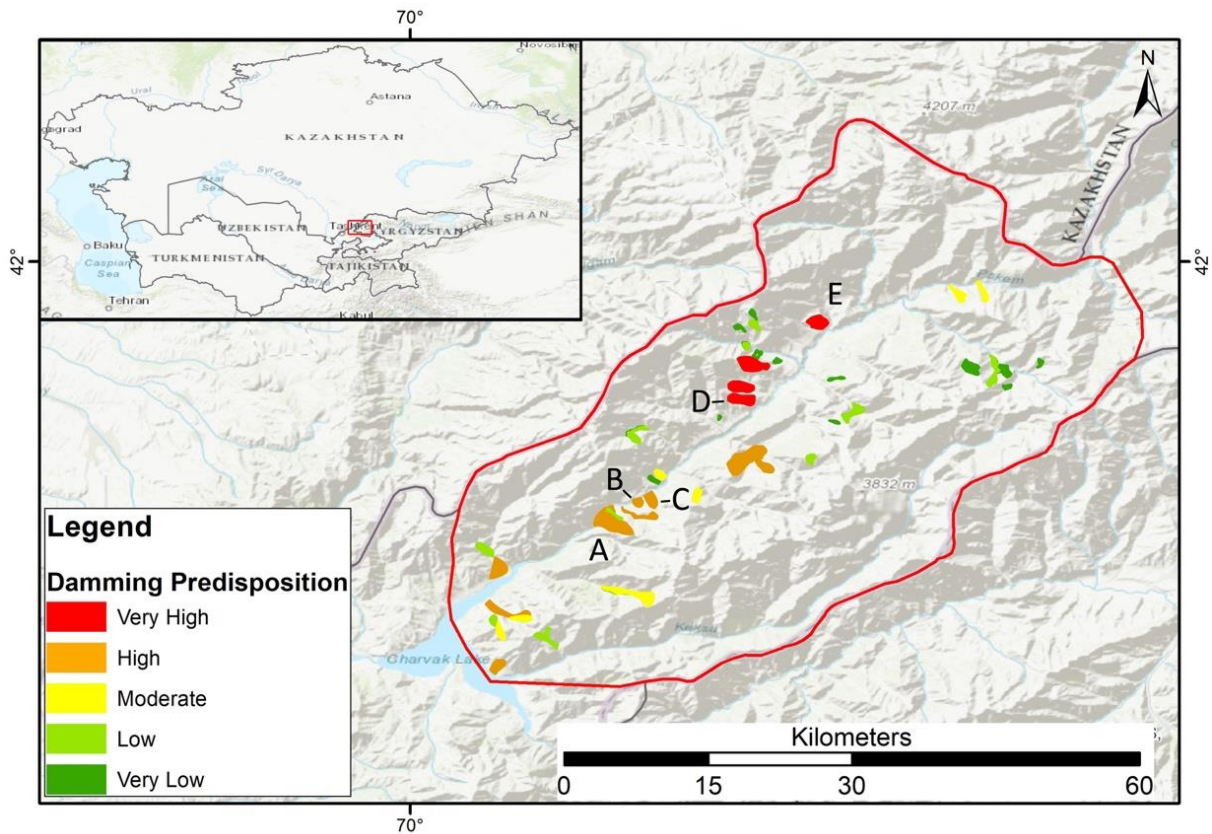
430 **4.1 Upper Pskem river valley (Uzbekistan)**

431 The Pskem river, locate in the Tashkent region of Uzbekistan, is a right-hand tributary of the Chirchik River that
 432 is the feeder of the Syr Darya river basin (in the Western Tien-Shan). The river originates from the confluence of
 433 the Maidantal and Oygaing rivers and is one of the main tributaries of the Charvak Lake (Semakova et al., 2016).
 434 This artificial lake is central for the local economy for its functions as reserve for fishing and water, as well as a
 435 source of hydroelectric energy and because of that various villages arise around it and downstream. The formation
 436 of a natural obstruction and an upstream impoundment in the Pskem basin could be a serious threat due to the
 437 possible instability of the earth dam and for the possible catastrophic cascade effects that its collapse could have
 438 downstream on the artificial basins and their 168 meters high earthfill dam.

439 With a careful observation of the map of Damming Predisposition by landslides reactivation in the lower Pskem
 440 basin in an area of 443 km² (Figure 23), some of the 53 mapped landslides should be subjected to further study.
 441 Among all, most landslides were classified with a Very Low and Low predisposition value, respectively 21 and
 442 11 cases (39.6% and 20.8%), and only 4 landslides with a Very High value (7.5%), 10 with High (18.9%) and 7
 443 with Moderate (13.2%). Landslides named A, B, C, D and E in Figure 23, if reactivated will potentially cause an
 444 obstruction of the main river section of the Pskem, being classified the first three and the latest two respectively
 445 with High and Very High damming predisposition. As shown in Table 2, the volumes of all these landslides are
 446 way bigger than the boundary volume of Non-Formation and Formation from Figure 24 and Figure 25. It is
 447 important to notice that the landslides A, B and C are laid down in the valley floor, meaning that in the past they
 448 had probably already dammed the river in that point, and the classification of their damming predisposition have
 449 been reduced by one, from Very High to High. Due to the considerable volumes of the landslides in the basin and
 450 the presence of landslides that have probably already blocked the river in the past, this relatively small area is
 451 certainly worthy of attention.

452 **Table 2. Landslides volumes and damming parameters W_v , V_1' , V_1'' of the landslides in Figure 20**
 453 **computed using the described method.**

Landslide	V_1 - Landslide volume (m ³)	W_v - River Width (m)	V_1' - Volume of Non-formation (m ³)	V_1'' - Volume of Formation (m ³)
A	200.000.000	300	2.600.000	16.200.000
B	12.000.000	235	1.500.000	10.000.000
C	34.000.000	318	3.000.000	18.200.000
D	73.000.000	513	10.100.000	47.400.000
E	61.000.000	575	13.500.000	60.000.000



454

455 **Figure 23. Map of Damming Predisposition by landslides reactivation in the lower Pskem basin.** Basemap
 456 source: Esri, HERE, Garmin Intermap, increment P Corp, GEBCO, USGS, FAO, NPS, NRCAN, GeoBase, IGN,
 457 Kadaster NL, Ordnance Survey, Esri Japan, METI, Esri China (Honk Kong), © OpenStreetMap contributors,
 458 and the GIS User Community.

459 The obstruction of the Pskem river by one of these landslides would cause an upstream impoundment with a
 460 surface from 2 to 10 km² or more, depending on the dam position and height. The dam collapse could release a
 461 catastrophic flooding wave with destructive effects in the downstream areas. In the worst scenario, even the
 462 earthfill dam located few kilometers downstream could be seriously damaged with unpredictable effects. Since the
 463 reliability of this mapping method is strictly correlated to the quality of the input data, when the used DEM has a
 464 coarse resolution, in similar cases of possible risk to people's life it is always advisable to do a second "manual
 465 check" even using some free satellite imaging services like Google Earth. In fact, when the DEM resolution is too
 466 rough, the GIS tool used in this methodology to evaluate the extension of the riverbed morphologic unit can

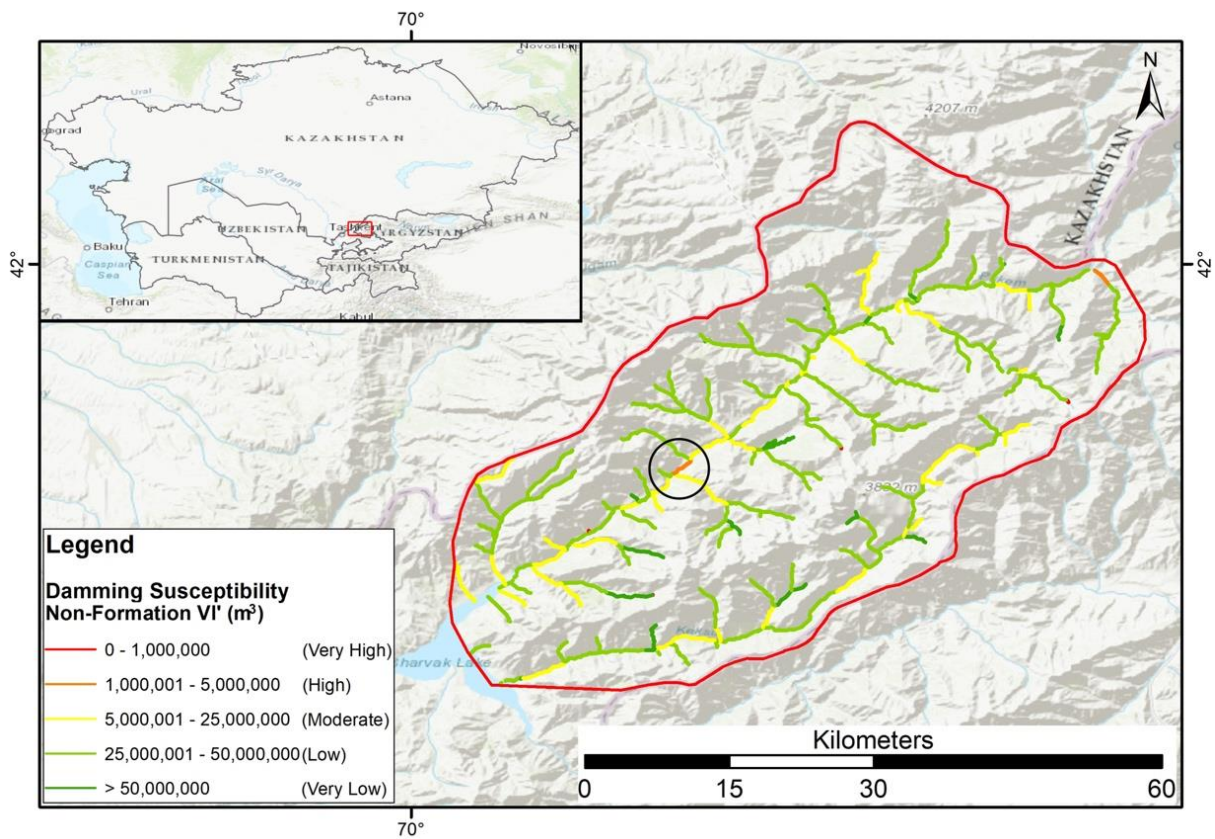
467 produce inconsistent and incorrect results, causing improper damming susceptibility evaluations. The results of
 468 the measurements on Google Earth orthophotos in Table 3 show that the difference between the river width values
 469 calculated with the mapping method (W_v) and those measured on Google Earth (W_{vGE}) can in some cases be
 470 substantial modifying the calculated boundary volumes V' and V'' , although in this case they do not modify
 471 drastically the final classification of the five landslides.

472 The river network of the upper Pskem valley have been also classified producing the maps of Damming
 473 Susceptibility of Non-formation and Formation (Figure 24 and Figure 25 respectively). Concerning the Damming
 474 Susceptibility Map of Non-formation (Figure 24), the most frequent are Low and Moderate classes with 65.1%
 475 and 22.6% respectively, followed by Very Low class with 11.1%. Only just 1.3% have been classified as High and
 476 0.0% as Very High. For the Damming Susceptibility Map of Formation (Figure 25) most of the rivers fall into
 477 Very Low and Low classes with 69.8% and 27.7%, followed by Moderate class with 2.1%. Only 0.4% have been
 478 classified as High and 0.0% as Very High.

479 **Table 3. Damming parameters W_{vGE} , $V_1'_{GE}$, $V_1''_{GE}$ of the landslides in Figure 23 computed with Google**
 480 **Earth observation.**

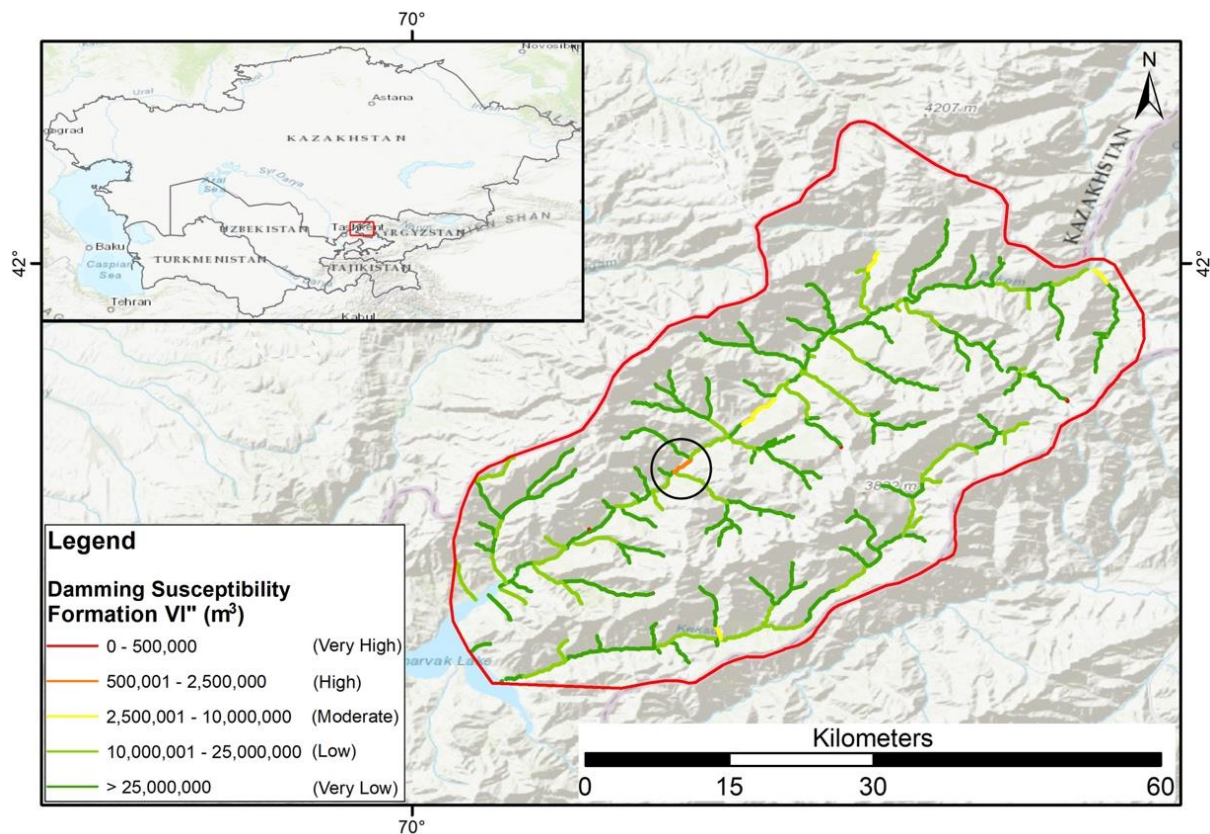
Landslide	W_{vGE} – River Width (m)	$V_1'_{GE}$ - Volume of non-formation (m ³)	$V_1''_{GE}$ - Volume of Formation (m ³)
A	415	6.000.000	31.000.000
B	310	2.800.000	17.300.000
C	260	1.800.000	12.100.000
D	530	11.000.000	50.000.000
E	450	7.300.000	36.500.000

481
 482 The general damming susceptibility of the valley is low but a singular river stretch, marked by a black circle in
 483 Figure 24 and Figure 25, classified with High susceptibility in both maps should be carefully evaluated. This river
 484 part is clearly noticeable in the middle of the area along the main river path, a bit upstream from the landslides
 485 named B and C. The high classification values mean that geographically in that point the valley width undergoes
 486 a shrinkage and for this reason even a relatively small landslide generated from the surrounding slopes can create
 487 an obstruction, therefore it would be worthy of a more detailed investigation.



488

489 **Figure 24. Damming Susceptibility Map of Non-formation of river stretches by new landslides in the lower**
 490 **Pskem basin. The black circle highlights a river stretch with unusually high values.** River network database
 491 from Coccia et al., (2023). Basemap source: Esri, HERE, Garmin Intermap, increment P Corp, GEBCO, USGS,
 492 FAO, NPS, NRCAN, GeoBase, IGN, Kadaster NL, Ordnance Survey, Esri Japan, METI, Esri China (Honk
 493 Kong), © OpenStreetMap contributors, and the GIS User Community.



494

495 **Figure 25. Damming Susceptibility Map of Formation of river stretches by new landslides in the lower**
 496 **Pskem basin. The black circle highlights a river stretch with unusually high values.** River network database
 497 from Coccia et al., (2023). Basemap source: Esri, HERE, Garmin Intermap, increment P Corp, GEBCO, USGS,
 498 FAO, NPS, NRCAN, GeoBase, IGN, Kadaster NL, Ordnance Survey, Esri Japan, METI, Esri China (Honk
 499 Kong), © OpenStreetMap contributors, and the GIS User Community.

500 4.2 The Fergana valley mountainous rim (Tajikistan-Kyrgyz Republic- 501 Uzbekistan)

502 The Fergana valley is one of the largest intermountain depressions in Central Asia located between Uzbekistan,
 503 Kyrgyz Republic, and Tajikistan. It hosts two main rivers, the Naryn and the Kara Darya, which join together to
 504 form the Syr Darya. In this populated area landslide activity is recurrent, causing every year damage to
 505 infrastructure and loss of human life, and triggered by complex interactions between multiple factors such as
 506 tectonic, geological, morphological and meteorological (Danneels et al., 2008; Schlögel et al., 2011; Piroton et al.,
 507 2020). The mapping methodology have been applied also to the Fergana valley and a total of 3370 landslides,
 508 coming from various data sources, have been classified as shown in Figure 26. Comparably to the classification
 509 result of the entire inventory (Figure 9) most of the cases (94%) have a Very Low damming predisposition,
 510 followed by Low and Moderate (with 2.5% and 1.8% respectively) as reported in Table 4. Just very few landslides
 511 fall into High and Very High classes (with 1.4% and 0.3% respectively). For the classification of the river network
 512 of the Fergana valley, the maps of Damming Susceptibility of Non-formation and Formation have been produced
 513 (Figure 27 and Figure 28 respectively). As a method with a multi-scale approach, in such large areas, this damming

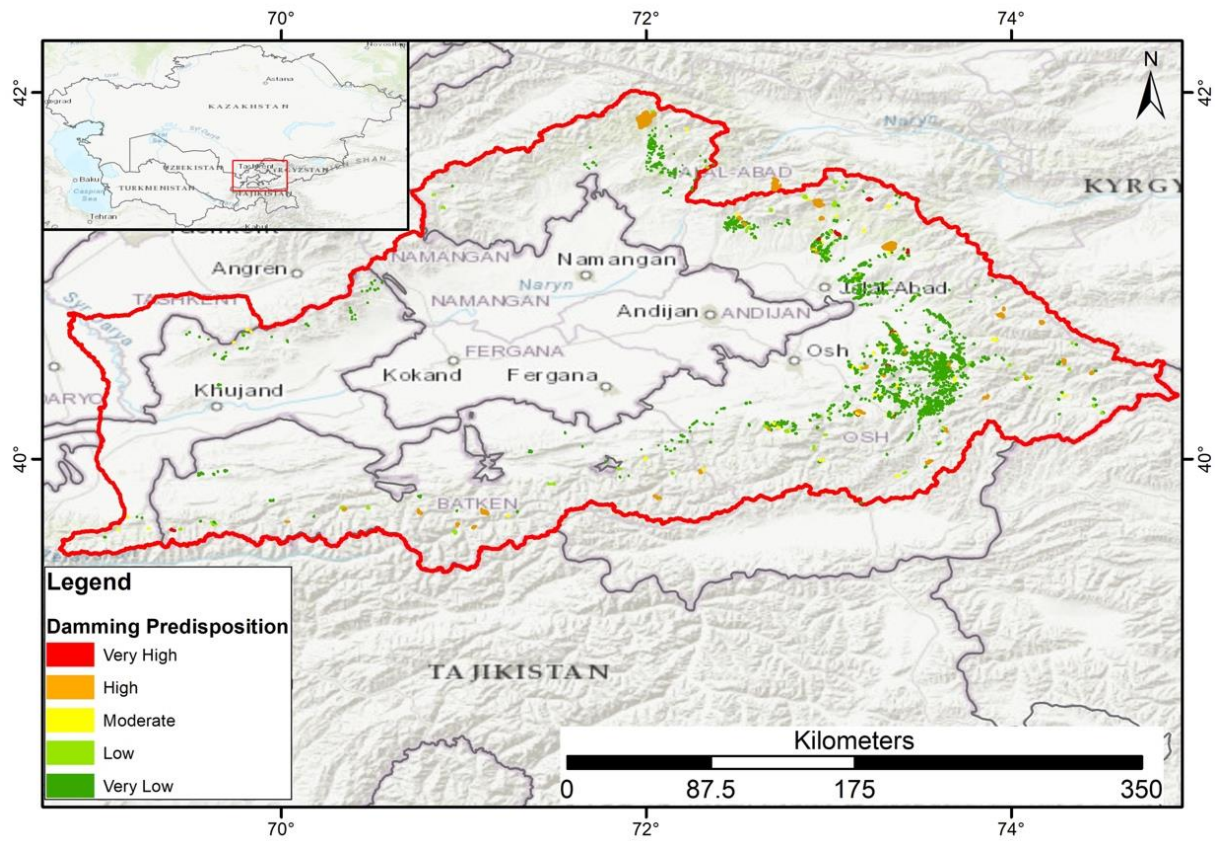
514 susceptibility method is suitable to provide territorial planning suggestions rather than indications on single
 515 interventions at local scale. The overall damming predisposition of the Fergana valley is quite low, considering
 516 the presence of 3370 mapped landslides in total, even if there are few landslides (10) classified with Very High
 517 damming predisposition which should be studied with more attention through localized analysis of damming
 518 susceptibility to ensure that downstream areas are not at risk and therefore require a specific monitoring.

519 Table 4 have been reported the distribution of the percentages of the damming susceptibility classes of those river
 520 stretches that are not running in flat areas, since these lowland rivers represent 53.6% of the total. Concerning the
 521 Damming Susceptibility Map of non-formation of the remaining river stretches (Figure 27), the most frequent are
 522 Low and Moderate classes with 53.4% and 36.2% respectively, followed by Very Low class with 7.0%. Only just
 523 2.1% and 1.3% have been classified as Very High and High. For the Damming Susceptibility Map of Formation
 524 (Figure 28) most of the rivers fall into Very Low and Low classes with 54.5% and 38.1%, followed by Moderate
 525 class with 5.2%. Only 1.9% and 0.2% have been classified as Very High and High respectively.

526 **Table 4. Distribution of Damming Susceptibility classes on existing landslides (Figure 26) and on the river**
 527 **stretches for non-formation (Figure 27) and Formation of new landslides (Figure 28).**

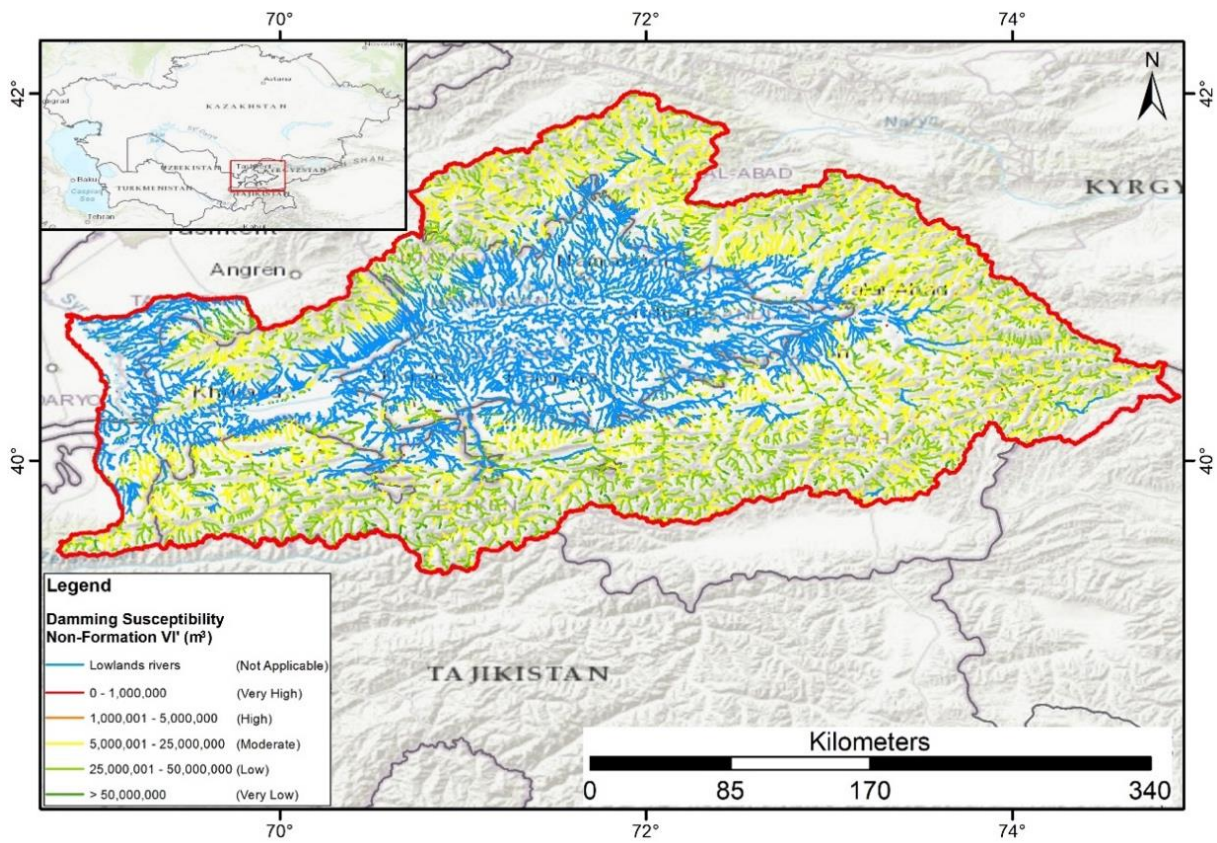
Damming Susceptibility	Landslides		non-formation	Formation
	n.	%	%	%
Very High	10	0.3%	1.9	1.7
High	48	1.4%	1.2	0.2
Moderate	61	1.8%	7.0	5.3
Low	83	2.5%	53.2	38.8
Very Low	3168	94.0%	6.7	54.0

528



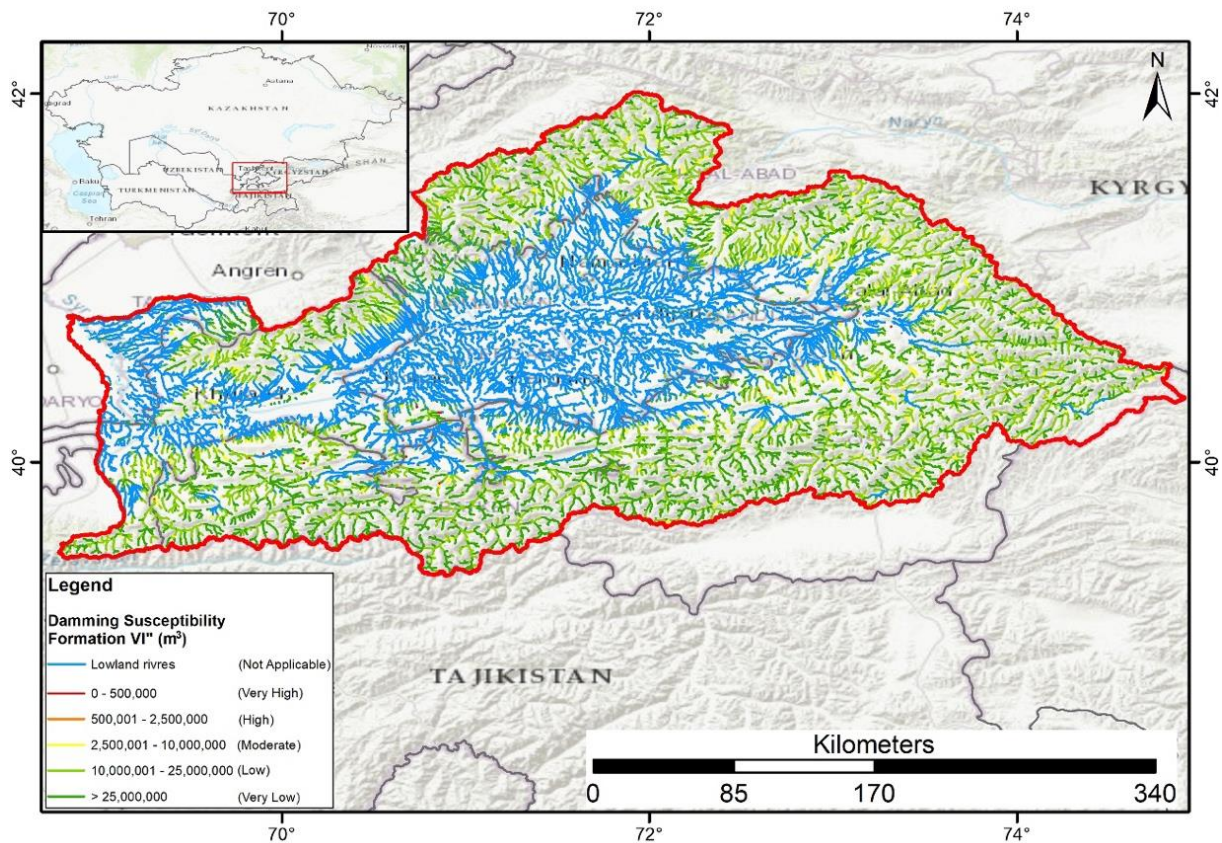
529

530 **Figure 26. Map of Damming Predisposition by landslides reactivation in the Fergana valley.** Basemap
 531 source: Esri, HERE, Garmin Intermap, increment P Corp, GEBCO, USGS, FAO, NPS, NRCAN, GeoBase, IGN,
 532 Kadaster NL, Ordnance Survey, Esri Japan, METI, Esri China (Honk Kong), © OpenStreetMap contributors,
 533 and the GIS User Community.



534

535 **Figure 27. Damming Susceptibility Map of Non-formation of river stretches by new landslides in the**
 536 **Fergana valley.** River network database from Coccia et al., (2023). Basemap source: Esri, HERE, Garmin
 537 Intermap, increment P Corp, GEBCO, USGS, FAO, NPS, NRCAN, GeoBase, IGN, Kadaster NL, Ordnance
 538 Survey, Esri Japan, METI, Esri China (Honk Kong), © OpenStreetMap contributors, and the GIS User
 539 Community.



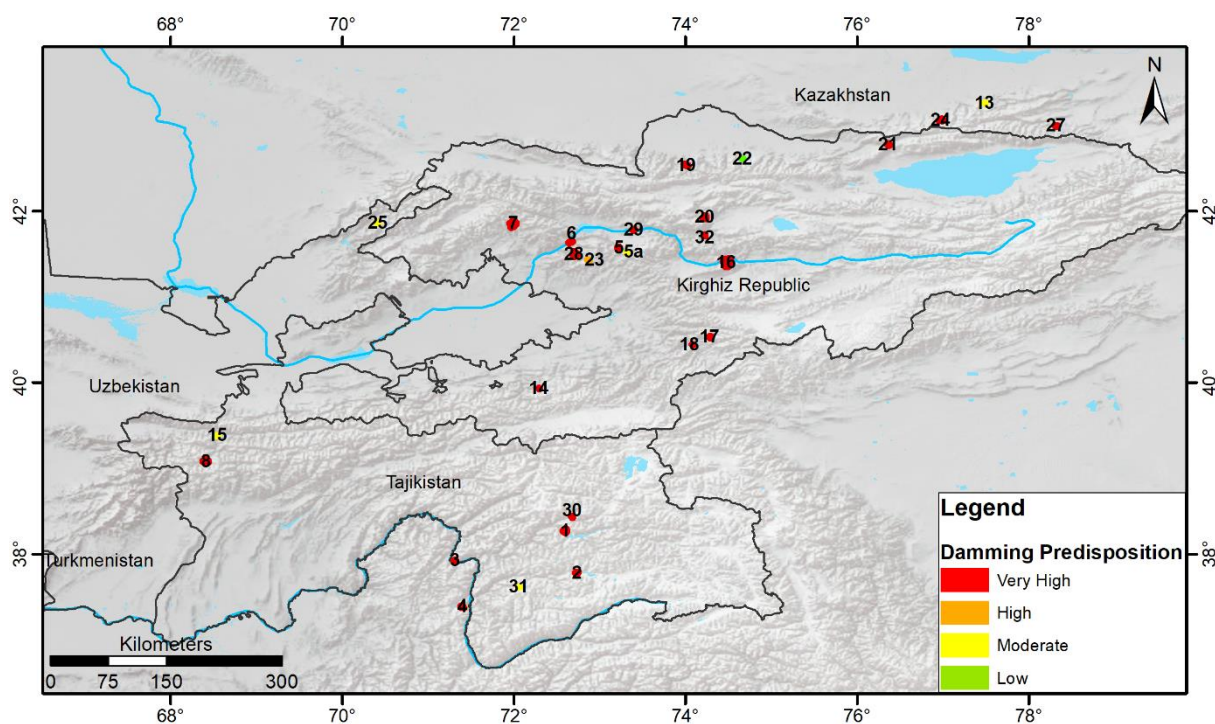
540

541 **Figure 28. Damming Susceptibility Map of Formation of river stretches by new landslides in the Fergana**
 542 **valley.** River network database from Coccia et al., (2023). Basemap source: Esri, HERE, Garmin Intermap,
 543 increment P Corp, GEBCO, USGS, FAO, NPS, NRCAN, GeoBase, IGN, Kadaster NL, Ordnance Survey, Esri
 544 Japan, METI, Esri China (Honk Kong), © OpenStreetMap contributors, and the GIS User Community.

545 **5 Discussion**

546 During the application of the damming mapping methodology, the main issues encountered was the extremely
 547 wide study area, the amount of data and the processing time required. The used mapping methodology based on
 548 the MOI equations (Eq.(1)), was originally designed to assess the damming susceptibility at basin/regional scale
 549 (Tacconi Stefanelli et al., 2016; 2020), where the morphological parameters essential for the correct application of
 550 the tool proposed by Wood (2009) must be correctly found to have an accurate river width required in the MOI
 551 equations (Eq.(1)). This time-consuming phase has been simplified in this research, according to the wide
 552 dimension of the study area, taking into account not the basins but the different states in the Central Asia region.
 553 This simplification certainly affected the reliability of the individual specific data, while still guaranteeing an
 554 important overview of the general hazard distribution of the phenomenon in the area. Furthermore, the results
 555 quality is directly proportional to the resolution and quality of the input data, which on the other hand is inversely
 556 proportional to the processing time. In this regard, a further criticality of this process is the reliability on the
 557 landslides volumes assessment method, since a higher quality of landslides data (sliding geometry and depth)
 558 allows the application of a more accurate volume calculation and therefore a better final result.

559 Considering the size of the area, in Figure 11 the number of landslides classified with Very High damming
 560 predisposition (166 cases) is reasonable in absolute value, even if a bit high if compared with the total number of
 561 landslides present in the inventory (8910 cases). Without a detailed study it is not possible to say how many of
 562 these are false positives or not, however it is important to remember that this type of hazard mapping methods
 563 gives information on if and where, not when these events may occur. Although a validation of all the results is
 564 not possible, we can verify some of these through comparison with cases known in the, as shown in Figure 29.
 565 These landslides have been documented in Strom (2010) who has reported several landslide dams in Central
 566 Asia regions. In Table 5 their current conditions are compared with their Damming Predisposition classification
 567 using the methodology proposed here (before the intensity reduction of the classification by one class of those
 568 landslides that intersect the river network). From this information can be observe that 23 (77% of the total) of
 569 these landslides were correctly classified with the Very High predisposition value, 1 (3%) as High and 5 (17%)
 570 with Moderate. Only one landslide, No. 22 called Arashan in Strom (2010), was classified as Low predisposition
 571 despite it obstructed the Alamedin River and then collapsed and deeply eroded. This classification error can be
 572 explained by the missing landslide volume eroded by the river as a bigger value would probably have provided a
 573 higher predisposition. Based on this simple comparison, approximately 80% of the landslide dams analysed by
 574 Strom (2010) has a corrected Damming Predisposition value (Very High) based on their volume and the width of
 575 their valley. The final classification value of Damming Predisposition of all of them has been downgraded by
 576 one class as they intersect the river network (see Section 3 Materials and Methods).



577
 578 **Figure 29. Map of Damming Predisposition using landslide from Strom (2010).** See Table 5 for landslide
 579 numbers. Lake's polygons from Esri, Garmin International, Inc.; basemap from Esri, USGS, NOAA.

580 **Table 5. Information of landslides in Figure 29 (from Strom, 2010) and their Damming Predisposition**
 581 **assessment.**

N.	Name	Mountain chain-Region	Consequences	Damming Predisposition
1	Usoi	Pamirs-Tajikistan	Dammed (with lake)	Very High
2	Yashilkul	Pamirs-Tajikistan	Dammed (with lake)	Very High
3	Shids	Pamirs-Tajikistan	Dammed (with lake, partially breached)	Very High
4	Shiva	Pamirs-Afghanistan	Dammed (with lake)	Very High
5	Karasu	Tien Shan-Kyrgyz Rep.	Dammed (with lake)	Very High
5a	Kapkatash	Tien Shan-Kyrgyz Rep.	Dammed (with lake)	Moderate
6	Karakul	Tien Shan-Kyrgyz Rep.	Dammed (filled lake)	Very High
7	Sarychelek	Tien Shan-Kyrgyz Rep.	Dammed (with lake)	Very High
8	Iskanderkul	Tien Shan-Tajikistan	Dammed (with lake)	Very High
9	Tianchi	Tien Shan-China	Dammed (with lake)	Very High
11	Twin-Lakes (upper)	Tien Shan-China	Dammed (with lake)	Very High
12	Twin-Lakes (lower)	Tien Shan-China	Dammed (with lake)	Very High
13	Issyk	Tien Shan-Kazakhstan	Dammed (with lake)	Moderate
14	Yashinkul	Tien Shan-Kyrgyz Rep.	Dammed (collapsed)	Very High
15	Aini	Tien Shan-Tajikistan	Dammed (lake artificially drained)	Moderate
16	Beshkiol	Tien Shan-Kyrgyz Rep.	Dammed (collapsed)	Very High
17	Kulun	Tien Shan-Kyrgyz Rep.	Dammed (with lake)	Very High
18	Kulun Mouth	Tien Shan-Kyrgyz Rep.	Dammed (filled lake)	Very High
19	Aksu	Tien Shan-Kyrgyz Rep.	Dammed (collapsed)	Very High
20	Kokomeren	Tien Shan-Kyrgyz Rep.	Dammed (collapsed)	Very High
21	Djashilkul	Tien Shan-Kyrgyz Rep.	Dammed (collapsed)	Very High
22	Arashan	Tien Shan-Kyrgyz Rep.	Dammed (collapsed)	Low
23	Kutmankul	Tien Shan-Kyrgyz Rep.	Dammed (with lake)	High
24	Bolshoe Almaty	Tien Shan-Kazakhstan	Dammed (with lake)	Very High
25	Badak	Tien Shan-Uzbekistan	Dammed (with lake)	Moderate
28	Dead Lakes	Tien Shan-Kyrgyz Rep.	Dammed (with lake)	Very High
29	Djuzumdybulak	Tien Shan-Kyrgyz Rep.	Dammed (with lake)	Very High
30	Kudara	Pamirs-Tajikistan	Dammed (collapsed)	Very High

31	Rivakkul	Pamirs-Tajikistan	Dammed (with lake)	Moderate
32	Ornok	Tien Shan-Kyrgyz Rep.	Dammed (collapsed)	Very High

582

583 The two maps of damming susceptibility (Figure 12 and Figure 15), while not providing probability values as done
584 by Tacconi Stefanelli et al. (2020), offer information (the volumes of landslides) that can be more easily spent and
585 interpreted even by operators who are not specifically expert, and for this reason have more practical utility.
586 Furthermore, the classification of the river stretches thus produced, not requiring the alpha parameter (linked to
587 the probability of landslide occurrence) as in the original method proposed by Tacconi Stefanelli et al. (2020), it
588 is much easier to obtain and for this reason it can be considered an improvement within a view of wider usability.

589 **6 Conclusions**

590 The price of a river obstruction, in terms of reconstruction and losses on both economic and lives, can be much
591 higher compared with the costs of a proper environmental planning and land-use management. Be able to define
592 the areas with higher risk could considerably lower the costs, allowing to focus the economic resources in effective
593 preventive interventions, planning and monitoring activities.

594 In this work a damming mapping methodology have been proposed and carried out on the Central Asia regions as
595 a part of a multi-hazard approach in the framework of the SFRARR Project (“Strengthening Financial Resilience
596 and Accelerating Risk Reduction in Central Asia”). The used method, originally developed applying the
597 Morphological Obstruction Index at basin scale, have been modified to fit such a large study area and the available
598 data. Over 8000 landslides and the entire river network of studied area have been analyzed to propose a practical
599 tool to assess where the damming susceptibility, from reactivation of mapped landslides and formation of new
600 landslides, are higher at national scale. The improvement of the original method allows a simpler use on a wider
601 area, as the technical knowledge and data required can also be managed by a non-expert operator, and the need for
602 less data, more easily available. The main limitation of the work is related to the uncertainty of the reliability of
603 the results at local scale due to the absence of a possible validation of all results, requiring many in-depth specific
604 studies in the areas identified with the higher predisposition. This uncertainty can be improved in future studies by
605 using data with better resolution, coverage, and quality.

606 Besides its limitations, this tool can be undoubted useful in very large countries where there is a lack of diffuse
607 assessment of landslide activity, providing preliminary information about damming susceptibility to adopt risk
608 reduction measures, for land management and as a starting point for future studies in specific areas potentially
609 more subject to the damming hazard identified in this work.

610 **Code and data availability.** The landslide dam mapping susceptibility method was implemented by using the cited
611 landslide inventory maps, published by the following authors: Behling et al., 2014, 2016, 2020; Havenith et al.,
612 2015a; Strom and Abdrakhmatov, 2018. The SRTM DEM data are available from <https://earthexplorer.usgs.gov/>.
613 The river network and other landslide inventories were provided by the SFRAAR project partners: RED (Risk,
614 Engineering + Development – Pavia, Italy), OGS (National Institute of Oceanography and Experimental
615 Geophysics, Seismological Research Center, Trieste, Italy), IWPHE (Institute of Water problems, Hydropower,
616 Engineering and Ecology, Dushanbe, Republic of Tajikistan), ISASUZ (Institute of Seismology of the Academy

617 of Science of Uzbekistan, Tashkent, Uzbekistan), LLP (Institute of Seismology of the Science Committee of the
618 Republic of Kazakhstan, Almaty).

619 **Author contribution.** Carlo Tacconi Stefanelli implemented the damming mapping method, William Frodella
620 conceived with Carlo Tacconi Stefanelli the article structure and collected the data, Francesco Caleca supported
621 the method application on part of the study area. Francesco Caleca also performed statistical analysis involving
622 the method results. All the aforementioned Authors contributed to the writing of the article and the figure graphics.
623 Veronica Tofani coordinated the work and reviewed the paper. Zhanar Raimbekova and Ruslan Umuraliev
624 provided environment and geomorphology information and part of the landslide database for Kazakhstan and
625 Kyrgyz Republic.

626 **Competing interests.** The contact author has declared that none of the authors has any competing interests.

627 **Acknowledgements.** This work was developed within World Bank-funded project “*Strengthening Financial*
628 *Resilience and Accelerating Risk Reduction in Central Asia*” (SFRARR), in collaboration with the European
629 Union, and the GFDRR (Global Facility for Disaster Reduction and Recovery), with the goal of improving
630 financial resilience and risk-informed investment planning in the central Asian countries (Kazakhstan, Kyrgyz
631 Republic, Tajikistan, Turkmenistan and Uzbekistan). This work brings the part of the results of the Task 7
632 “Landslide Scenario Assessment”, managed by the UNESCO Chair on Prevention and Sustainable Management
633 of Geo-Hydrological Hazards (University of Florence, Italy). In particular, the authors would like to thank Gabriele
634 Coccia and Paola Ceresa from Red Risk Engineering (Pavia, Italy) for providing river network data and for the
635 valuable coordination and constant support, and also Alexander Strom and Hans Balder Havenith for providing
636 landslide inventories and for their constructive advice and valuable observations. We would also like to thank the
637 partners from Central Asia for the fruitful collaboration, in particular: IWPHE (Tajikistan), ISASUZ and the State
638 Monitoring Service of the Republic of Uzbekistan for tracking dangerous geological processes (Uzbekistan), the
639 Institute of Seismology of the National Academy of Sciences of Kyrgyz Republic (ISNASKR), and the Institute
640 of Seismology Limited Liability Partnership (LLP) of Kazakhstan.

641 **Financial support.** This research has been supported by the World Bank Group (Consulting Services Contract No.
642 8006611 – Regionally consistent risk assessment for earthquakes and floods and selective landslide scenario
643 analysis for strengthening financial resilience and accelerating risk reduction in Central Asia).

644 **References**

645 Abdrakhmatov, K.Y., Aldazhanov, S.A., Hager, B.H., Hamburger, M.W., Herring, T.A., Kalabaev, K.B.,
646 Makarov, P. Molnar, S.V. Panasyuk, M.T. Prilepin, R.E. Reilinger, I.S. Sadybakasov, B.J. Souter, Yu.A.
647 Trapeznikov, V.Ye., and Tsurkov Zubovich, A.V.: Relatively recent construction of the Tien Shan inferred
648 from GPS measurements of present-day crustal deformation rates. *Nature*, 384(6608), 450-45319, 1996.

649 Abdrakhmatov, K., Havenith, H.B., Delvaux, D., Jongmans, D., and Trefois, P.: Probabilistic PGA and Arias
650 Intensity Maps of Kyrgyz Republic (Central Asia). *J. Seismol.* 7.2: 203-220, 2003.

651 Behling, R., Roessner, S., Kaufmann, H., and Kleinschmit, B.: Automated spatiotemporal landslide mapping over
652 large areas using rapideye time series data. *Remote Sens.* 6, 8026–8055, 2014.

653 Behling, R., Roessner, S., Golovko, D., and Kleinschmit, B.: Derivation of long-term spatiotemporal landslide
654 activity—A multi-sensor time series approach. *Remote Sens. Environ.* 186, 88–104, 2016.

655 Behling, R., and Roessner, S.: Multi-temporal landslide inventory for a study area in Southern Kyrgyz Republic
656 derived from RapidEye satellite time series data (2009 – 2013). V. 1.0. GFZ Data Services.
657 <https://doi.org/10.5880/GFZ.1.4.2020.001>, 2020.

658 Borgatti, L., and Soldati, M.: Landslides as a geomorphological proxy for climate change: a record from the
659 Dolomites (northern Italy), *Geomorphology*, 120(1–2), 56–64, 2010.

660 CAC DRMI: Risk assessment for Central Asia and Caucasus: desk study review, 2009.

661 Canuti, P., Casagli, N., Ermini, L., Fanti, R., and Farina, P.: Landslide activity as a geoinicator in Italy:
662 significance and new perspectives from remote sensing, *Environ. Geol.*, 45(7), 907–919, 2004.

663 Casagli, N., and Ermini, L.: Geomorphic analysis of landslide dams in the Northern Apennine, *Trans. Jpn.*
664 *Geomorphol. Union.*, 20(3), 219–249, 1999.

665 Catani, F., Tofani, V., and Lagomarsino, D.: Spatial patterns of landslide dimension: a tool for magnitude mapping,
666 *Geomorphology* 273, 361–373. <https://doi.org/10.1016/j.geomorph.2016.08.032>, 2016.

667 Chedia, O.K., and Lemzin, I.N.: Seismogenerating faults of the Chatkal depression. In: *Seismotectonics and*
668 *seismicity of the Tien Shan*. Frunze, Ilim, 18–28, 1980.

669 Chen, C. Y., Chang, J. M.: Landslide dam formation susceptibility analysis based on geomorphic features.
670 *Landslides*, 13(5), 1019-1033, 2016.

671 Coccia, G., Ceresa, P., Bussi, G., Denaro, S., Bazzurro, P., Martina, M., Fagà, E., Avelar, C., Ordaz, M., Huerta,
672 B., Garay, O., Raimbekova, Z., Abdrakhmatov, K., Mirzokhonova, S., Ismailov, V., and Belikov, V.: Large-
673 scale flood risk assessment in data scarce areas: an application to Central Asia, *Nat. Hazards Earth Syst. Sci.*
674 *Discuss.* [preprint], <https://doi.org/10.5194/nhess-2023-157>, in review, 2023.

675 Costa, J.E., and Schuster, R.L.: Documented historical landslide dams from around the world. *US Geol. Surv.*
676 *Open-File Report*, 91(239), 1-486, 1991.

677 Costa, J.E., and Schuster, R.L.: Formation and failure of natural dams. *Bull Geol Soc Am*, 100 (7), 1054–1068.
678 [https://doi.org/10.0016-1988\)100/0016-7606\(1988\)100<1054:TFAFON>2.3.CO](https://doi.org/10.0016-1988)100/0016-7606(1988)100<1054:TFAFON>2.3.CO), 1988.

679 Crozier, M.J.: Deciphering the effect of climate change on landslide activity: a review, *Geomorphology*, 124(3),
680 260–267, 2010.

681 Dai, F. C., Lee, C. F., Deng, J. H., Tham, L. G.: The 1786 earthquake-triggered landslide dam and subsequent
682 dam-break flood on the Dadu River, southwestern China. *Geomorphology*, 65(3), 205-221, 2005.

683 Dal Sasso, S.F., Sole, A., Pascale, S., Sdao, F., Bateman Pinzòn, A., and Medina, V.: Assessment methodology
684 for the prediction of landslide dam hazard, *Nat. Hazards Earth Syst. Sci.*, 14 (3), 557–567,
685 <http://dx.doi.org/10.5194/nhess-14-557-2014>, 2014.

686 Danneels, G., Bourdeau, C., Torgoev, I., Havenith, H. B. Geophysical investigation and dynamic modelling of
687 unstable slopes: case-study of Kainama (Kyrgyzstan). *Geophys. J. Int.*, 175(1), 17-34, 2008.

688 Delvaux, D., Abdrakhmatov, K.E., Lemzin, I.N., and Strom, A.L.: Landslides and surface breaks of the 1911 Ms
689 8.2 Kemin earthquake, Kyrgyzstan, *Russian Geology and Geophysics*, 2001, 42, 10, 1667-1677, 2001.

690 Dikau, R., and Schrott, L.: The temporal stability and activity of landslides in Europe with respect to climatic
691 change (TESLEC): main objectives and results, *Geomorphology*, 30(1–2), 1–12, 1999.

692 Drăguț, L., and Dornik, A.: Land-surface segmentation as a method to create strata for spatial sampling and its
693 potential for digital soil mapping, *Int. J. Geogr. Inf. Sci.*, 30(7), 1359-1376, 2016.

694 Ermini, L., Casagli, N.: Prediction of the behavior of landslide dams using a geomorphical dimensionless index,
695 *Earth Surf Proc Land* 28:31–47. <https://doi.org/10.1002/esp.424>, 2003.

696 Falátková, K.: Temporal analysis of GLOFs in high-mountain regions of Asia and assessment of their causes,
697 *AUC Geographica*, 51, 2, 145–154, 2016.

698 Fan, X., Rossiter, D.G., van Westen, C.J., Xu, Q., and Görüm, T.: Empirical prediction of coseismic landslide dam
699 formation, *Earth. Surf. Proc. Land.*, 39(14), 1913–1926, 2014.

700 Fan, X., Dufresne, A., Subramanian, S.S., Strom, A., Hermanns, R., Tacconi Stefanelli, C., Hewitt, K., Yunus,
701 A.P., Dunning, S., Capra, L., Geertsema, M., Miller, B., Casagli, N., Jansen, J.D., and Xu, Q.: The formation
702 and impact of landslide dams – State of the art, *Earth Sci. Rev.*, 203, 103116,
703 <https://doi.org/10.1016/j.earscirev.2020.103116>, 2020.

704 Fan, X., Dufresne, A., Whiteley, J., Yunus, A. P., Subramanian, S.S., Okeke, C. A., Pánek, T., Hermanns, R.,
705 Ming, P., Strom, A., Havenith, H.-B., Dunning, S., Wang, G., and Tacconi Stefanelli, C.: Recent
706 technological and methodological advances for the investigation of landslide dams, *Earth-Sci. Rev.*, 218,
707 103646, <https://doi.org/10.1016/j.earscirev.2021.103646>, 2021.

708 Farr, T.G., and Kobrick, M.: Shuttle Radar Topography Mission produces a wealth of data. *Eos Trans. AGU*, 81,
709 583-583, 2000.

710 Golovko, D., Roessner, S., Behling, R., Wetzel, H. U., and Kleinschmidt, B.: Development of multi-temporal
711 landslide inventory information system for southern Kyrgyz Republic using GIS and satellite remote sensing,
712 *PFG*, 2015(2), 157–172, 2015.

713 Guzzetti, F., Ardizzone, F., Cardinali, M., Rossi, M., and Valigi, D.: Landslide volumes and landslide mobilization
714 rates in Umbria, central Italy, *EPSL*, 279, 222–229, 2009.

715 Havenith, H.B., Strom, A., Cacerez, F., and Pirard, E.: Analysis of landslide susceptibility in the Suusamyр region,
716 Tien Shan: statistical and geotechnical approach. *Landslides* 3, 39–50, 2006a.

717 Havenith, H.B., Torgoev, I., Meleshko, A., Alioshin, Y., Torgoev, A., and Danneels, G.: Landslides in the Mailuu-
718 Suu Valley, Kyrgyz Republic—hazards and impacts, *Landslides*, 3, 137–147, 2006b.

719 Havenith, H.B., Strom, A., Torgoev, I., Torgoev, A., Lamair, L., Ischuk, A., and Abdrakhmatov, K.: Tien Shan
720 geohazards database: Earthquakes and landslides, *Geomorphology*, 249, 16–31, 2015a.

721 Havenith, H.B., Torgoev, A., Schlögel, R., Braun, A., Torgoev, I., and Ischuk, A.: Tien Shan geohazards database:
722 Landslide susceptibility analysis, *Geomorphology*, 249, 32–43, 2015b.

723 Havenith, H.B., Umaraliev, R., Schlögel, R., Torgoev, I., Ruslan, U., Schlogel, R., and Torgoev, I.: Past and
724 Potential Future Socioeconomic Impacts of Environmental Hazards in Kyrgyz Republic. In *Kyrgyz Republic:
725 Political, Economic and Social Issues*; Olivier, A.P., Ed.; Nova Science Publishers, Inc.: Hauppauge, NY,
726 USA; pp. 63–113, 2017.

727 Hungr, O., and Evans, S.G.: Entrainment of debris in rock avalanches: an analysis of a long run-out mechanism,
728 *Geol. Soc. Am. Bull.*, 116(9-10), 1240-1252, 2004.

729 Juliev, M., Pulatov, A., and Hubl, J.: Natural hazards in mountain regions of Uzbekistan: A review of mass
730 movement processes in Tashkent province. *International Journal of Scientific and Engineering Research*,
731 8(2), 1102, 2017.

732 Kalmetieva, Z.A., Mikolaichuk, A.V., Moldobekov, B.D., Meleshko, A. V, Janaev, M.M., and Zubovich, A.V.:
733 Atlas of earthquakes in Kyrgyz Republic. Central-Asian Institute for Applied Geosciences and United
734 Nations International Strategy for Disaster Reduction Secretariat Office in Central Asia, Bishkek, p 75, 2009.

735 King, J., Loveday, I., Schuster, R. L.: The 1985 Bairaman landslide dam and resulting debris flow, Papua New
736 Guinea. *Q J Eng Geol Hydroge*, 22(4), 257-270, 1989.

737 Kropáček, J., Vilímek, V. & Mehrishi, P.: A preliminary assessment of the Chamoli rock and ice avalanche in the
738 Indian Himalayas by remote sensing, *Landslides*, 18, 3489–3497, [https://doi.org/10.1007/s10346-021-
739 01742-1](https://doi.org/10.1007/s10346-021-01742-1), 2021.

740 Liao, H. M., Yang, X. G., Lu, G. D., Tao, J., and Zhou, J. W.: A geotechnical index for landslide dam stability
741 assessment, *Geomatics, Natural Hazards and Risk*, 13(1), 854-876,
742 <https://doi.org/10.1080/19475705.2022.2048906>, 2022.

743 Maxwell, A.E., and Shobe, C.M.: Land-surface parameters for spatial predictive mapping and modeling, *Earth-
744 Sci. Rev.*, 226, 103944, 2022.

745 Molnar, P., and Tapponnier, P.: Cenozoic Tectonics of Asia: Effects of a Continental Collision: Features of recent
746 continental tectonics in Asia can be interpreted as results of the India-Eurasia collision. *science*, 189(4201),
747 419-426, 1975.

748 Niyazov, R.A.: Uzbekistan landslides. Uzbekistan landslide service. Technical report, 2020.

749 Peresan, A., Scaini, C., Tyagunov, S., and Ceresa, P.: Capacity Building Experience for Disaster Risk Reduction
750 in Central Asia, *Nat. Hazards Earth Syst. Sci. Discuss.* [preprint], <https://doi.org/10.5194/nhess-2023-156>, in
751 review, 2023.

752 Petrov, M.A., Sabitov, T.Y., Tomashevskaya, I.G., Glazirin, G.E., Chernomorets, S.S., Savernyuk, E.A.,
753 Tutubalina O.V., Petrakov, D.A., Sokolov, L.S., Dokukin, M.D., Mountrakis, G., Ruiz-Villanueva, V., and
754 Stoffel, M.: Glacial lake inventory and lake outburst potential in Uzbekistan, *Sci. Total Environ.*, 592, 228-
755 242, 2017.

756 Piroton, V., Schlögel, R., Barbier, C., and Havenith, H.B.: Monitoring the recent activity of landslides in the
757 Mailuu-suu valley (Kyrgyz Republic) using radar and optical remote sensing techniques. *Geosciences*, 10
758 (5), p. 164, 2020.

759 Popescu, M.E., and Sasahara, K.: Engineering Measures for Landslide Disaster Mitigation, in: *Landslides –*
760 *Disaster Risk Reduction*, edited by: Sassa, K., Canuti, P., Springer, Berlin, Heidelberg, 609-631,
761 https://doi.org/10.1007/978-3-540-69970-5_32, 2009.

762 Righini, M., and Surian, N.: Remote sensing as a tool for analysing channel dynamics and geomorphic effects of
763 floods, *Flood monitoring through remote sensing*, 27-59, 2018.

764 Rosi, A., Frodella, W., Nocentini, N., Caleca, F., Havenith, H.B., Strom, A., Saidov, M., Bimurzaev, G.A., and
765 Tofani, V.: Comprehensive landslide susceptibility map of Central Asia, *Nat. Hazards Earth Syst. Sci.*, 23,
766 2229–2250, <https://doi.org/10.5194/nhess-23-2229-2023>, 2023.

767 Saponaro, A., Pilz, M., Wieland, M., Bindi, D., Moldobekov, B., and Parolai, S.: Landslide susceptibility analysis
768 in data-scarce regions: the case of Kyrgyz Republic. *Bull. Eng. Geol. Environ.* 74, 1117–1136, 2014.

769 Schlögel, R., Torgoev, I., De, Marneffe, C., and Havenith, H.B.: Evidence of a changing size-frequency
770 distribution of landslides in the Kyrgyz Tien Shan, Central Asia. *Earth Surf Process Landf* 36(12), 1658–
771 1669, 2011.

772 Schuster, R.L., and Evans, S.G.: Engineering Measures for the Hazard Reduction of Landslide Dams, in: *Natural*
773 *and Artificial Rockslide Dams. Lecture Notes in Earth Sciences*, edited by: Evans, S., Hermanns, R., Strom,
774 A., Scarascia-Mugnozza, G., Springer, Berlin, Heidelberg, https://doi.org/10.1007/978-3-642-04764-0_2,
775 2011.

776 Semakova, E., Gunasekara, K., and Semakov, D.: Identification of the glaciers and mountain naturally dammed
777 lakes in the Pskem, the Kashkadarya and the Surhandarya River basins, Uzbekistan, using ALOS satellite
778 data, *Geomat. Nat. Hazards Risk*, 7(3), 1081-1098, 2016.

779 Strom, A.: Landslide dams in Central Asia region. *Journal of the Japan Landslide Society*, 47(6), 309-324, 2010.

780 Strom, A., and Abdrakhmatov, K.: Large-Scale Rockslide Inventories: From the Kokomeren River Basin to the
781 Entire Central Asia Region (WCoE 2014–2017, IPL-106-2, in: *Workshop on World Landslide Forum*.
782 Springer, Cham, pp. 339–346, 2017.

783 Strom, A., and Abdrakhmatov, K.: Rockslides and rock avalanches of Central Asia: distribution, morphology, and
784 internal structure. Elsevier, 441pg. ISBN: 978-0-12-803204-6, 2018.

785 Swanson, F.J., Oyagi, N., and Tominaga, M.: Landslide dams in Japan, in: *Landslide dams: processes, risk and*
786 *mitigation*, vol 3, edited by: Schuster R.L., Geotech. Sp., ASCE, New York, 131–145, 1986.

787 Tacconi Stefanelli, C., Catani, F., Casagli, N.: Geomorphological investigations on landslide dams. *Geoenviron Disast*
788 2(1):1–15. <https://doi.org/10.1186/s40677-015-0030-9>, 2015.

789 Tacconi Stefanelli, C., Segoni, S., Casagli, N., and Catani, F.: Geomorphic indexing of landslide dams evolution,
790 *Eng. Geol.*, 208, 1–10. <https://doi.org/10.1016/j.enggeo.2016.04.024>, 2016.

791 Tacconi Stefanelli, C., Vilfimek, V., Emmer, A., and Catani, F.: Morphological analysis and features of the
792 landslide dams in the Cordillera Blanca, Peru, *Landslides*, 15(3), 507-521, [https://doi.org/10.1007/s10346-](https://doi.org/10.1007/s10346-017-0909-5)
793 [017-0909-5](https://doi.org/10.1007/s10346-017-0909-5), 2018.

794 Tacconi Stefanelli, C., Casagli, N., and Catani, F.: Landslide damming hazard susceptibility maps: a new GIS-
795 based procedure for risk management, *Landslides*, 17, 1635-1648, [https://doi.org/10.1007/s10346-020-](https://doi.org/10.1007/s10346-020-01395-6)
796 [01395-6](https://doi.org/10.1007/s10346-020-01395-6), 2020.

797 Trifonov, V.G., Makarov, V.I., and Scobelev, S.F.: The Talas-Fergana active right-slip faults. *Ann Tectonicae*
798 6:224–237, 1992.

799 Ullah, S., Bindi, D., Pilz, M., Danciu, L., Weatherill, G., Zuccolo, E., Anatoly Ischuk, A., Mikhailova, N.N.,
800 Abdrakhmatov, K., and Parolai, S. Probabilistic seismic hazard assessment for Central Asia. *Annals of*
801 *Geophysics*, 58(1), 2015.

802 Wang, X., Ding, Y., Liu, S., Jiang, L., Wu, K., Jiang, Z., and Guo, W.: Changes of glacial lakes and implications
803 in Tian Shan, central Asia, based on remote sensing data from 1990 to 2010, *Environ. Res. Lett.*, 8(4),
804 044052, 2013.

805 Wang, D., Laffan, S.W., Liu, and Y., and Wu, L.: Morphometric characterization of landform from DEMs, *Int. J.*
806 *Geogr. Inf. Sci.*, 24(2), 305–326, 2010.

807 Wood, J.: Geomorphometry in LandSerf. In: Hengl, T. and Reuter, H.I. [Eds.]: *Geomorphometry: Concepts,*
808 *Software, Applications*, *Dev. Soil. Sci.*, 33, 333-349, 2009.

809 Zubovich, A. V., Wang, X. Q., Scherba, Y. G., Schelochkov, G. G., Reilinger, R., Reigber, C., Mosienko, O.,
810 Molnar, P., Michajljow, W., Makarov, V.I., Li, J., Kuzikov, S.I., Herring, T.A., Hamburger, M.W., Hager
811 B.H., Dang, Y., Bragin, V.D., and Beisenbaev, R.: GPS velocity field for the Tien Shan and surrounding
812 regions. *Tectonics*, 29(6), 2010.